Metallurgical Failure Analysis of C-130 Part Number 372903-1R T9936A

Dr. R.A. Saravanan

Center for Aircraft Structural Life Extension (CAStLE)
Department of Engineering Mechanics

United States Air Force Academy
Colorado Springs, Colorado 80840

September 2004

APPROVED FOR PUBLIC RELEASE; DISTRIBUTION UNLIMITED

DEAN OF THE FACULTY
UNITED STATES AIR FORCE ACADEMY
COLORADO 80840

USAFA-TR-04-06

This technical report, Metallurgical Failure Analysis of C-130 Part Number 372903-1R T9936A, is presented as a competent treatment of the subject, worthy of publication. The United States Air Force Academy vouches for the quality of the research, without necessarily endorsing the opinions and conclusions of the authors. Therefore, the views expressed in this article are those of the authors and do not reflect the official policy or position of the United States Air Force, Department of Defense, or the US Government.

This report has been cleared for open publication and public release by the appropriate Office of Information in accordance with AFI 61-202 and USAFA FOI 190-1. This report may have unlimited distribution.

18 October 2004
Date

Dr. R.A. Saravanan
Senior Failure Analysis Engineer,
Center for Aircraft Structural Life Extension

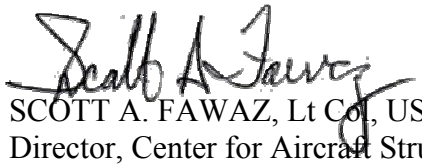

19 October 2004
Date

SCOTT A. FAWAZ, Lt Col, USAF
Director, Center for Aircraft Structural Life Extension

Quad Chart

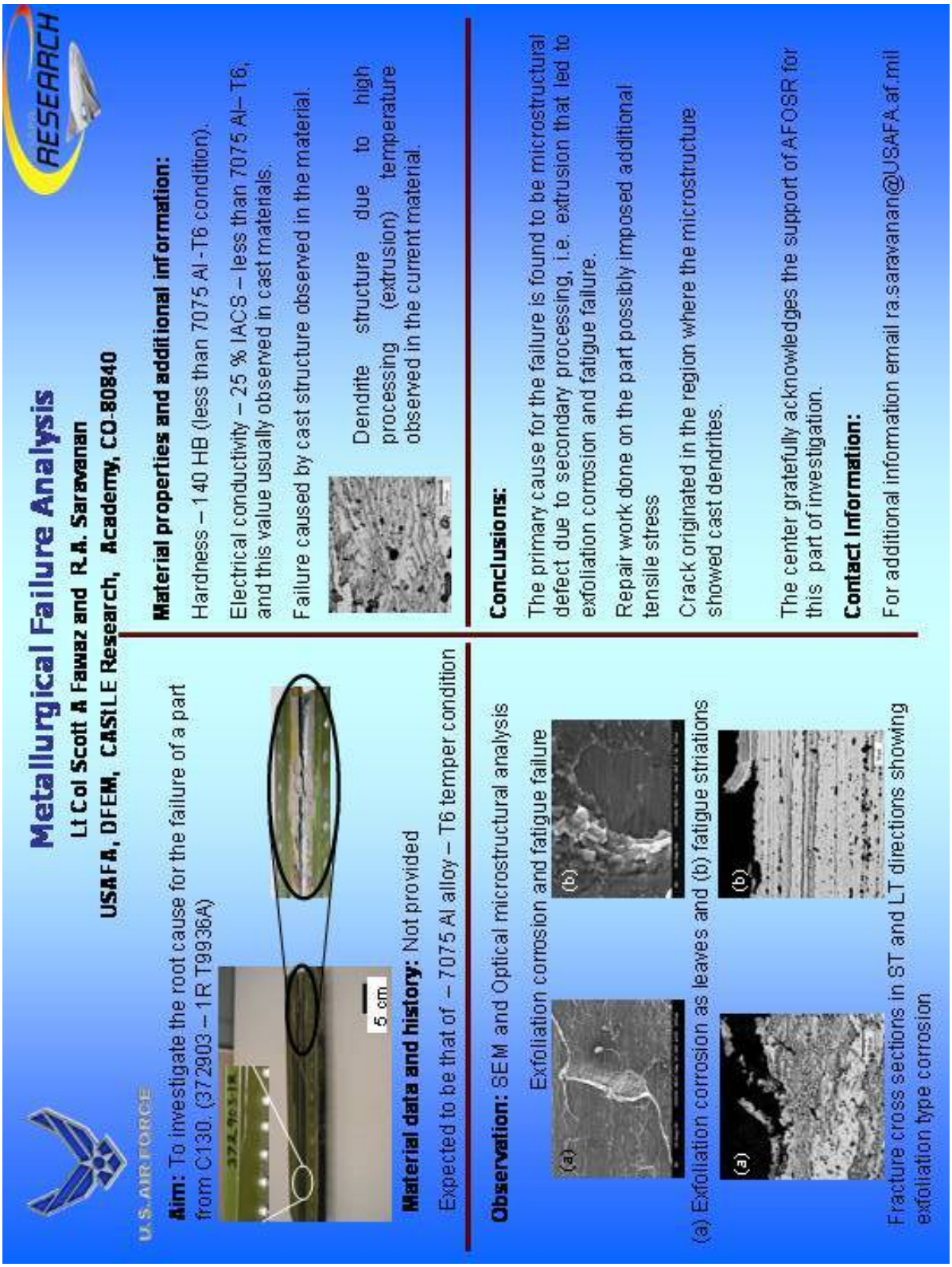
Metallurgical Failure Analysis
Lt Col Scott A Fawaz and R.A. Saravanan
USAFA, DFEM, CASILE Research, Academy, CO-80840
RESEARCH
U.S. AIR FORCE
Aim: To investigate the root cause for the failure of a part from C130. (372903 – 1R T9936A)
5 cm
Material data and history: Not provided
Expected to be that of – 7075 Al alloy – T6 temper condition
Material properties and additional information:
Hardness – 140 HB (less than 7075 Al-T6 condition).
Electrical conductivity – 25 % IACS – less than 7075 Al– T6; and this value usually observed in cast materials.
Failure caused by cast structure observed in the material.
Dendrite structure due to high processing (extrusion) temperature observed in the current material.
Observation: SEM and Optical microstructural analysis
Exfoliation corrosion and fatigue failure
(a)
(b)
(a) Exfoliation corrosion as leaves and (b) fatigue striations
(a)
(b)
Fracture cross sections in ST and LT directions showing exfoliation type corrosion
Conclusions:
The primary cause for the failure is found to be microstructural defect due to secondary processing, i.e. extrusion that led to exfoliation corrosion and fatigue failure.
Repair work done on the part possibly imposed additional tensile stress
Crack originated in the region where the microstructure showed cast dendrites.
The center gratefully acknowledges the support of AFOSR for this part of investigation.
Contact Information:
For additional information email ra.saravanan@USAFA.af.mil

Metallurgical Failure Analysis Summary

1. Organization: HQ USAFA/DFEM Center for Aircraft Structural Life Extension 2354 Fairchild Drive, Suite 2J2, USAF Academy, CO 80840	**2. Customer:** Mr. Peter Christiansen WR – ALC/LB **Contact Person:**
3. Date: Date Received: Unknown Date completed: 09/06/04	**4. Contact Person/ Investigator:** Scott A. Fawaz, Lt Col, USAF Dr. R.A. Saravanan
5. Part Number: 372903-1R T9936A, from C130	
6. Report Number: CAStLE-04-C130-01	**File Number:** C130-01-04
5. Failure analysis: Macroscopic - Yes Optical Microscopy - Yes SEM - Yes Hardness - Yes Tensile data - No Electrical conductivity - Yes	**6. Material History:** No
7. Determination of the root cause for the failure/Reason: a) Complete - √ b) Partial c) Incomplete	
8. Recommendations if any: - None	
9. Comments: - Subject to the more evidence or history regarding the repair and processing history, further discussion could be included.	
Report Prepared by: R. A. Saravanan	**Approved by:** Scott A. Fawaz

Abstract

Metallurgical failure analysis of the part received from a C-130 (372903 -1R T9936A) shows extensive damage due to exfoliation corrosion and high cycle fatigue. The primary cause for the failure is found to be microstructural defects due to secondary processing, i.e. extrusion that led to exfoliation corrosion and fatigue failure. Presence of both fine recrystallized grain in the outer edge (near the extrusion die contact) as well as cast structure (in the thick and central area) showed clear evidence regarding the metallurgical problem associate with processing. As a consequence, at least this part has failed due to exfoliation corrosion, initiated in the area where the cast structure is present. Intergranular corrosion, which is a severe form of exfoliation, is due to the presence of intermetallic inclusions and precipitates along the inter-dendrites. SEM and EDAX analysis were done on both fracture surfaces as well as on the sub-surfaces, whereas optical microscopy, hardness and electrical conductivity measurements were done on the cross section of the fracture surface and region away from the fracture surface. Evidence of exfoliation intergranular corrosion in the form of leaves and etching of grain boundaries were visible in the SEM fracture surface analysis. The striations due to fatigue were mostly damaged due to corrosion and their products. Additional evidence and information on the failure analysis are provided in Appendixes at the end of the report.

Table of Contents

Quad Chart ii
Metallurgical Failure Analysis Summary iii
Abstract iv
Table of Contents v
List of Figures vi
List of Tables viii
1. Introduction 1
2. Macroscopic Analysis 2
3. SEM Observation 6
4. Optical Microstructural Analysis 11
5. Hardness and Electrical Conductivity Measurements 17
6. Conclusion 17
7. References 18
Appendix A: Supplemental Images 19
Appendix B: EDAX Data 20
Appendix C: SEM micrographs after cleaning with Alconax 23
Appendix D: Component Schematics 25
Appendix E: Photomicrographs of Polished and Etched Specimens. 26
Appendix F: Variation in the grain size though the section thickness 28

List of Figures

Figure 1: (a) Macroscopic image of the part taken using a digital camera (inset shows the crack tip) and (b) Zoomed image of the section showing repair and fracture surface smearing seen as dark spots (arrow show the dark spots). 2
Figure 2: Macroscopic image of the part as seen from the top and dotted line show section made before opening the crack. 3
Figure 3: Image taken at 20x showing location of the crack tip, and sectioning by white lines. White arrows show the loading direction for crack opening. 3
Figure 4: (a) Zone 1 (refer Figure 7) of the fractured surface with sealant (outlined by blue line), and (b) sealant in the section about 5 cm (1.96 in) away from the front end. Marker "A" indicates smeared fracture surface, "B" corrosion products and "C" salt deposits and (c) Enlarged view of a region with massive salt deposits shown by arrow. 4
Figure 5: (a) and (b) shows evidence of exfoliation in the form of leaves as observed on the fracture surface, (c) and (d) shows evidence of exfoliation in the form delamination as observed from the sides (beyond the sealant region). 5
Figure 6: (a) Low magnification image of the sealant that appears as fatigue failure with striations and (b) high magnification of the striations in a stereo-microscope appears as small particles possibly because of broken pieces of polymeric chain (resin). 6
Figure 7: Schematic fracture part and sectioning. "Zone 1" is the fracture initiation part. 7
Figure 8: SEM Micrograph of the fracture surfaces: (a, b) taken at low and high magnification from Zone 1: (c, d) Zone 2 and zone 4 respectively, and (e) Zone end region where the crack was opened, and (f) Low magnification (corrosion and overload stress rupture region). "LT" represent longitudinal transverse direction. 8
Figure 9: Possible fatigue striations observed in zone 2 - 5: (a) Striations partially covered by corrosion products, striations shown by arrows; (b) high magnification of the same region, and (c) striations observed in zone 2 surface extensively damaged by oxides... 13
Figure 10: High magnification from (a) corroded region and (b) overload stress rupture. 13
Figure 11: SEM micrograph of the Alocnax cleaned fracture surface taken from (a) zone-2 and (b) Zone-4 clearly shows multiple leaves either partially or completely broken, and several intergranular cracks. Arrow indicates the grain boundary separation region during intergranular fracture. And (c, d) fatigue striations exposed after Alconax cleaning. 14
Figure 12: A 3D view of the microstructure with its orientation. 15
Figure 13: (a) Low and (b) high magnification optical microstructure in LT directions shows intermetallic inclusions aligned in the extrusion direction and in the intergranular region. Inclusion particle in the triple junction, is shown inside circles 15
Figure 14: (a) Low and (b) high magnification optical microstructure in LS directions shows intermetallic inclusions aligned in the extrusion direction and in the intergranular region. 16
Figure 15: (a) Low and (b) high magnification optical microstructure in ST directions shows intermetallic inclusions aligned in the extrusion direction and in the intergranular region 16
Figure A 1: Multiple cracks observed in the as received part are shown below prior to cutting the parts. 19
Figure A 2: Exfoliation additional photomicrographs 19

Figure B 1: The SEM micrograph shows the cross section of the fracture surface with clear exfoliation type corrosion. High magnification of the rectangular box represents the region from where the area analysis was done. Circular region shows the region where the subsequent analysis was done. 20
Figure B 2: EDAX spot analysis taken on a crack below the fracture surface. SEM micrograph shows the cross section of the fracture surface at high magnification. EDAX analysis was done in crack tip below the fracture surface. Cross symbol represents the spot analysis area. The exact location of this crack is shown in the previous micrograph as a circular region. 21
Figure B 3: EDAX spot analysis taken on the fracture surface. SEM micrograph shows the cross section of the fracture surface. EDAX analysis is taken on the fracture top surface. Cross symbol represents the spot analysis area. 22
Figure C 1: SEM micrographs of the fracture surface after cleaning with Alconax are shown below from Zone 2. 23
Figure C 2: SEM micrographs of the fracture surface after cleaning with Alconax are shown below from Zone 4. Arrows indicates the intergranular region attacked severely by corrosion environment. The corrosion products are completely etched by cleaning in Alconax solution. Compare these micrographs with Figure 8 (b & d). 24
Figure D 1: Schematic sectioning from the sample for optical microscopy. 25
Figure D 2: Schematic of repair and possible imposition of tensile stress from the additional plate and support. Microstructural analysis of the circular region is given in Appendix F. 25
Figure E 1: Leaves seen in the cross section of the fracture surface in ST direction. 26
Figure E 2: Leaves seen in cross section of the fracture surface in LT direction. 26
Figure E 3: Cross section of the fracture surface in ST direction. Dendritic structure is clearly visible even at low magnification. 27
Figure E 4: Intergranular corrosion running along the inter-dendrite region. 27
Figure F 1: Micrograph of circular region from Figure D2 indicating regions in subsequent micrographs from this Appendix. 28
Figure F 2: Region 1- low and high magnification optical micrographs near the edge where there is large strain due to contact with die. 28
Figure F 3: Optical micrographs of a) Region 2 b) Region 3 and c, d) Region 4 as described by Figure F1. 29
Figure F 4: Optical micrographs of Region 4 - high magnification. 30

List of Tables

Table 1. Hardness data measured from sectioned specimen and compared with standard 17
Table 2. Electrical conductivity measured from sectioned specimen and compared with standard. 17

1. Introduction

1.1 Description:

Not available

1.2 Material Requirement:

This part is expected to be made of AA7075 – T6

1.3 Background:

The part received is not provided with any background information and history. However, from the visual examination, it could be clearly seen some repair work has already been done on this part that did not benefit from arresting the crack.

1.4 Aim:

The purpose of this investigation is to determine the root cause of the failure.

2. Macroscopic Analysis

2.1 Macroscopic observation

The part received from the C-130 is expected to be made from AA7075 - T6. Macroscopic images were taken prior to cutting the part using a digital camera. Care was taken not to rub the fractured parts or disturb the fractured surfaces. Figure 1a shows macroscopic image of the part prior to cutting and Figure 1b an enlargement of a section where a repair was done with arrows showing regions of dark spots, a possible location of fracture smearing. In addition, a small inset shows an enlargement of a section where the crack terminates. Visual observation clearly reveals that the part was subjected to repair using some kind of sealant. In the later stage of the analysis, it was evident that the part was cracked and repaired using what appears to be aluminum sheet attached with rivets and faz sealant, and supported using a similar part by rivets. It should be noted here that the support material did not fail or show evidence of cracking.

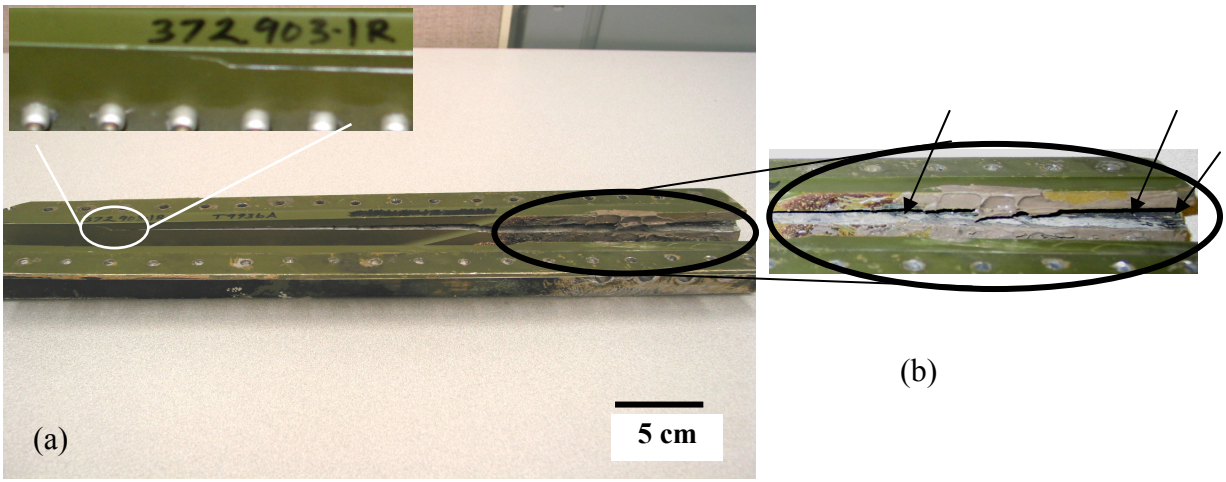

Figure 1: (a) Macroscopic image of the part taken using a digital camera (inset shows the crack tip) and (b) Zoomed image of the section showing repair and fracture surface smearing seen as dark spots (arrow show the dark spots).

Though the supporting material did not fail, presumably this particular part was removed or sectioned for failure investigation due to long crack propagation, and presence of multiple cracks that would have caused a threat to the structural integrity of the part. Images of the other cracks found in the as received part are given in ***Appendix A***.

2.2 Crack Opening

A sequential procedure was followed in sectioning the part and opening the crack are described below. Preliminary marks were made on the part using a permanent marker based on the total length of part. The overall length of the part is about 42 cm (16.54 in) and it is divided in 8 sections. The first two sections where approximately of equal spacing of about 2 cm (0.787 in), sections 3, 4 where approximately 5 cm (1.96 in), and 10 cm (3.94 in)respectively: and, sections 5-8 where approximately of equal spacing of about 5.75 cm (2.26 in). Though, the part was marked for sectioning it was decided to make judgment regarding the exact locations after opening the crack.

The part was sectioned using a band saw on the dotted line as shown in Figure 2. After sectioning the part, the location of the tip of the crack was identified for crack opening. A permanent marker pen was used to paint the surface near the end of the crack and later wiped with alcohol. With the help of a stereo-microscope, the crack tip was identified without much difficulties and the position is marked using a fine tip marker pen. Figure 3 shows the location of the crack tip by a black dot, and "V" marker position for cutting the part for crack opening. The part was cut on the "V" mark and the crack was opened by applying a load manually in the arrow direction specified in the figure 3.

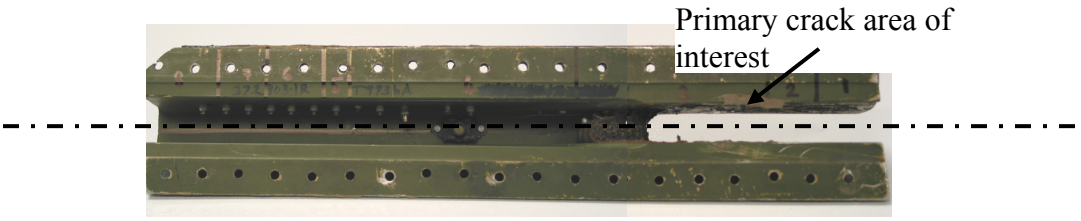

Figure 2: Macroscopic image of the part as seen from the top and dotted line show section made before opening the crack.

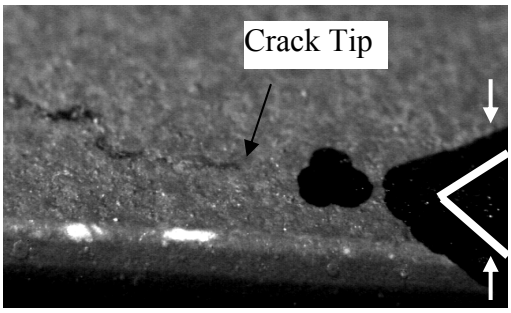

Figure 3: Image taken at 20x showing location of the crack tip, and sectioning by white lines. White arrows show the loading direction for crack opening.

2.3 Stereo-microscopic observation on the fracture surface:

Macroscopic observation using a stereo-microscope was carried out prior to sectioning the part for SEM (Scanning electron microscopy) observation. From the observation of the fracture surface and near surfaces under the stereo-microscope, at least 3 major features were observed:

1. Presence of sealant on the fracture surface observed for about 8 cm (3.15 in).
2. Presence of salts and corrosion products on the fracture surface. Composition analysis using EDAX (Energy Dispersive X-ray analysis) in SEM was used in the later stage to confirm their presence.
3. Evidence of exfoliation corrosion

The presence of sealant observed only near the initial section of the part running a length of about 8 cm (3.15 in) indicates that the part was subjected to repair work. Later the crack propagated to a span of approximately 38 cm (13.9 in) during service, where in these regions no sealant was observed. Figure 4(a-c) shows the evidence of the sealant, corrosion products and salt deposits.

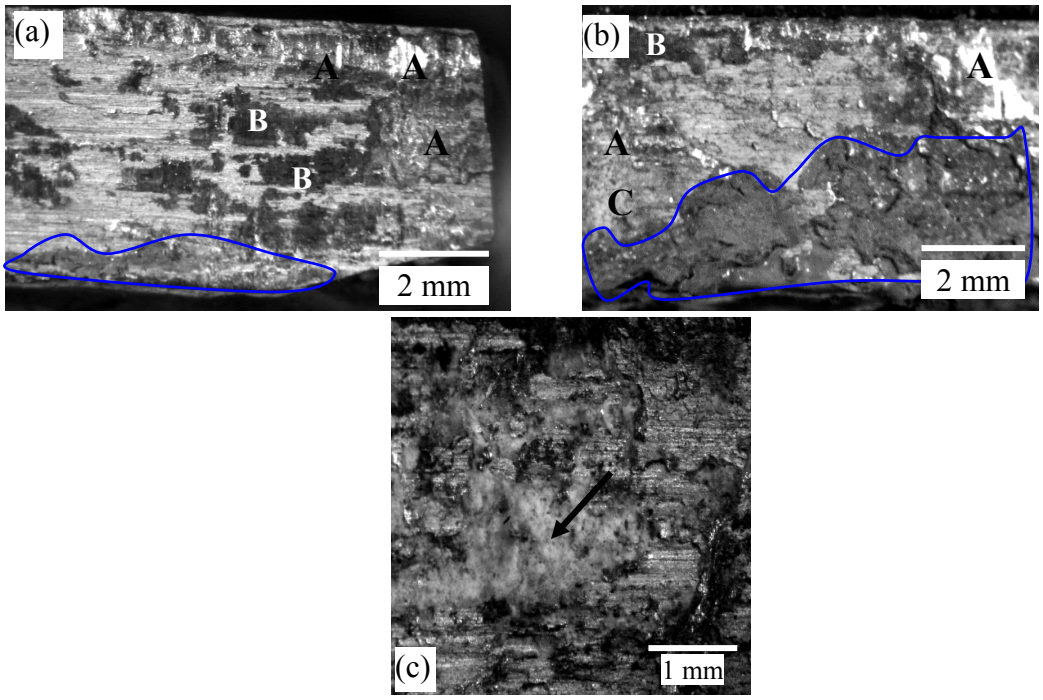

Figure 4: (a) Zone 1 (refer Figure 7) of the fractured surface with sealant (outlined by blue line), and (b) sealant in the section about 5 cm (1.96 in) away from the front end. Marker "A" indicates smeared fracture surface, "B" corrosion products and "C" salt deposits and (c) Enlarged view of a region with massive salt deposits shown by arrow.

Stereo-microscopic observation on the fractured surface and on the sides reveals evidence of exfoliation corrosion. Figure 5 (a-b) shows the exfoliation in the form of leaves on the fractured surface in both sealant region (a) and beyond sealant region (b). Figure 5 (c-d) shows the exfoliation seen as delamination of layers from the sides. Additional pictures showing delamination layers or cracks are provided in the ***Appendix A***. It was difficult to observe the delaminated layers on sides in the sealant region as they were all covered with sealant.

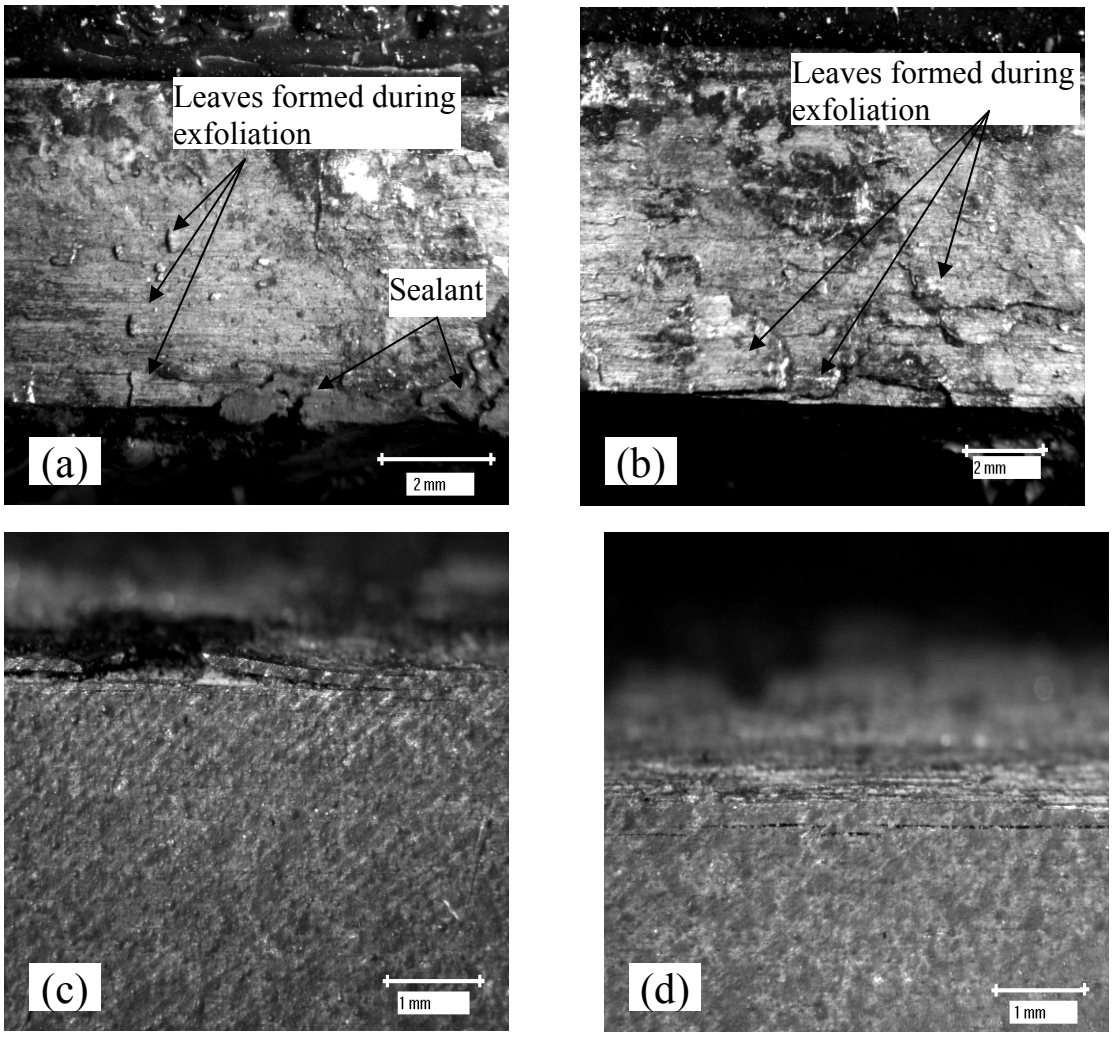

Figure 5: (a) and (b) shows evidence of exfoliation in the form of leaves as observed on the fracture surface, (c) and (d) shows evidence of exfoliation in the form delamination as observed from the sides (beyond the sealant region).

Macroscopic investigation thus indicates exfoliation corrosion as the main cause both in the sealant region as well as away from the sealant region. However, finer details like whether the cracks propagated due to stress or fatigue corrosion, it is premature to say unless supported by

SEM analysis. Conclusion made that repair work was done prior to the major cracking is based on the failure nature of the sealant as shown in Figure 6 (a, b) (otherwise sealant surface would appear smooth). It should be noted here that though the sealant appears to white in the Figure 6 (a & b), visual examination shows the sealants are dark brown or black in color and it appears as white due to illumination under stereomicroscope at an oblique angle.

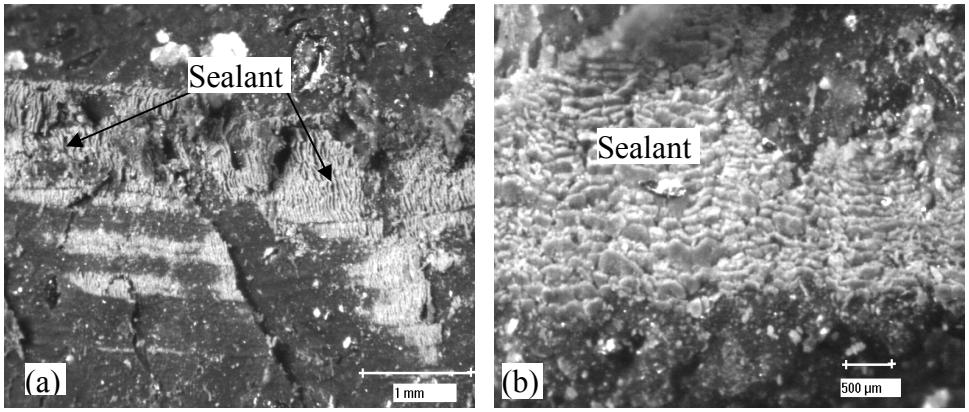

Figure 6: (a) Low magnification image of the sealant that appears as fatigue failure with striations and (b) high magnification of the striations in a stereo-microscope appears as small particles possibly because of broken pieces of polymeric chain (resin).

3. SEM Observation

SEM and EDAX (Energy Dispersive X-ray Analysis) analysis were done on the fracture surface after sectioning the part as mentioned in the earlier section. The part was cut into several subsections using a band saw, will now be referred as zone. Figure 7 show a schematic of the fracture surface, sectioning and the notation used in the text. The surfaces were observed without cleaning or removing the corroded products or salts, however they were thoroughly cleaned using compressed nitrogen gas to remove any dust or lose debris that would contaminate the SEM chamber. After initial observation, the fracture surfaces were also cleaned using Alconax solution (15g in 350 ml water, preheated to 95 ºC and ultrasonically cleaned for 30 min), then thoroughly washed in water and alcohol. Secondary electron image and EDAX analysis were carried out only on the fracture surface without cleaning with Alconax. This is due to the fact that cleaning with Alconax would remove the corroded products and etch the surface and EDAX analysis will not provide any evidence of corrosion products.

3.1 General Observation (prior to cleaning with Alconax solution)

SEM micrographs taken from the different zones are shown in figures 8a to 8f. In general, all the zones except the "zone end" were strongly affected by corrosion, probably exfoliation. The whole fracture surface except the over load rupture - zone end was found corroded, severely oxidized and finer details were not clearly identified. At higher magnification the fracture surface appeared as if they are totally covered with some oxides as shown in figures 8b, 8d, or 10a. The only feature that was clearly distinguishable was intergranualar corroded region with deep grooves along the LT directions and in some locations they were also covered with oxidizes. Since the features observed at different zones were almost same, especially "zone 2" to "zone 5", discussion will be made only for "zone 1", "zone 2- 5" and "zone end".

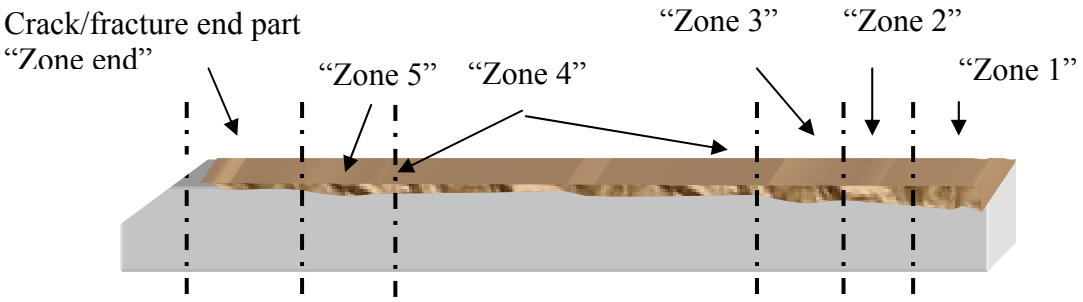

Figure 7: Schematic fracture part and sectioning. "Zone 1" is the fracture initiation part.

3.1.1 Zone 1

Evidence of exfoliation in zone 1 in the form of leaves was not observed, probably due to surface damage caused by smearing either during transport or repair. However, presences of deep grooves in the intergranular region running along the LT direction suggest the exfoliation type corrosion (Fig. 8b).

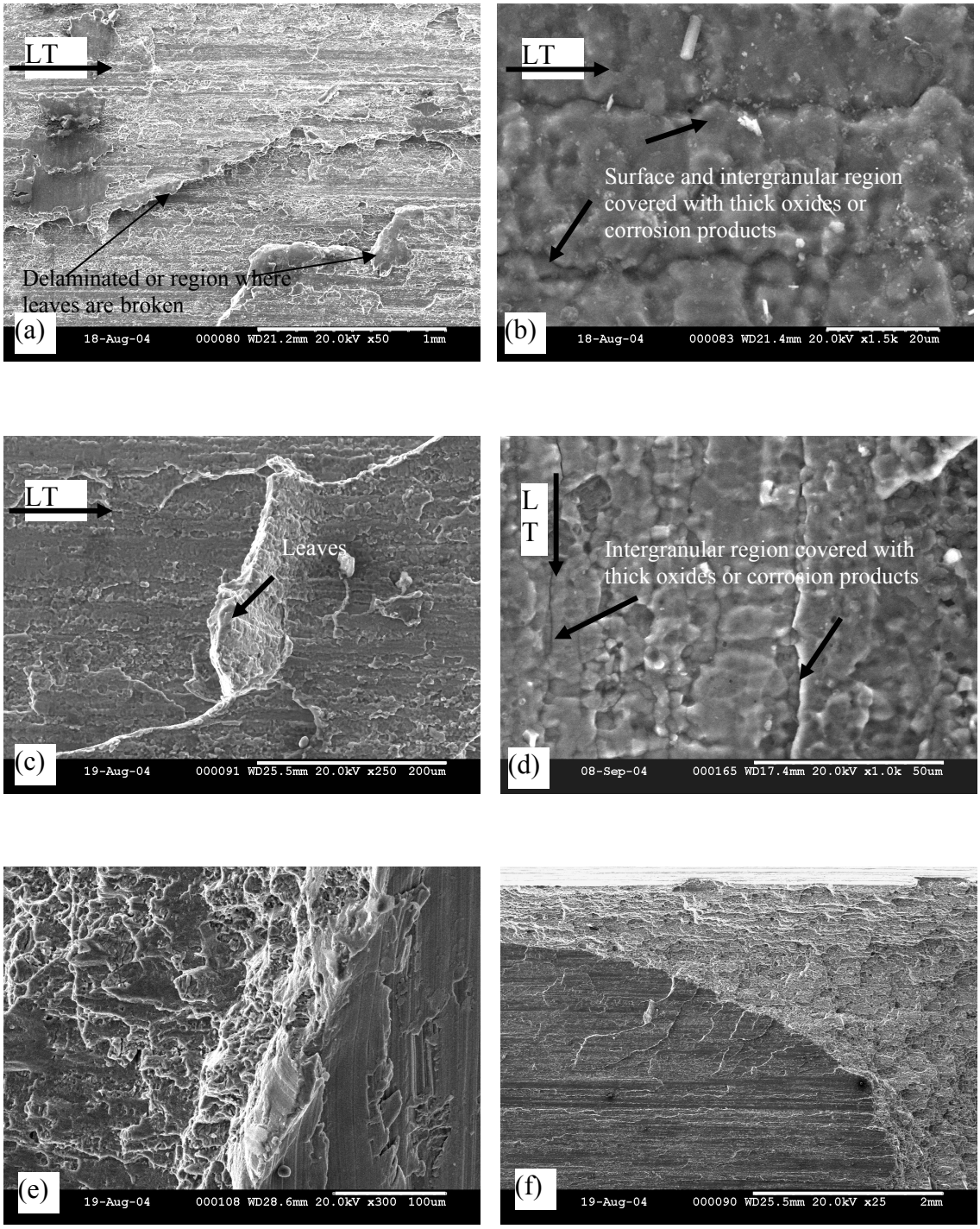

Figure 8: SEM Micrograph of the fracture surfaces: (a, b) taken at low and high magnification from Zone 1: (c, d) Zone 2 and zone 4 respectively, and (e) Zone end region where the crack was opened, and (f) Low magnification (corrosion and overload stress rupture region). "LT" represent longitudinal transverse direction.

3.1.2 Zone 2 – 5

In this zone, leaves formed during exfoliation corrosion were observed as shown in Figure 8c. The surfaces were covered with oxides or corroded products as in the case of Zone 1, and the surface damage due to smear/rubbing was not observed. To identify the corrosion product entrapped below the leaves, samples from these zones were sectioned in the LT direction and mounted. The mounted samples were then polished and SEM and EDAX analysis were done on the corrosion products that showed large deposits of sodium, sulfur and oxygen. EDAX analysis and their images are given in ***Appendix B***.

Effort was made to locate the service history like fatigue. As mentioned earlier, it was difficult to clearly locate the fatigue striations as the surfaces were covered with oxides or corrosion products. However, in some regions there were faint indications of striations indicating the part experienced fatigue loading during service and the crack propagated by fatigue as well. Figure 9 (a-c) shows region where there are some indications of fatigue. As can be seen in Figure 9a, part of the striations are still covered by oxides or corrosion products; in other words, a thin patch of oxide partially removed or detached from the surface exposing faint striation marks. Higher magnification of Figure 9a mainly the area containing striations are shown in Figure 9b. The fact the striations lye below the oxidation/corroded products clears the ambiguity whether striations are artifact due to rubbing or actual fatigue striations. Figure 9c shows a similar region, where the striations are badly damaged due to rubbing (presence of grooves and lips shown by arrow due to abrasion of hard particles possibly debris from the surface) suggest that possibility of artifact cannot be ruled out in this case.

3.1.3 Zone end

Figure 8(e, f) and 10(a, b) shows the SEM micrographs taken from the zone end. The region where the actual crack terminated and then was opened by cutting the “V” groove can be seen in Figure 8e, and Figure 8f show the transition from fracture mode from the one assisted by corrosion to tensile overload fracture or stress rupture. Figure 10a is much similar to the zone 2-5 where the fracture surface is covered with oxides and a clear intergranular crack with brittle mode of fracture could be seen.

Cleaved facets of intermetallic particles/inclusions are surrounded by fine shallow dimples which is typical of tensile overload fracture are clearly seen in figure 10b. These inclusions are rich in iron and the silicon is weakly bonded to the matrix. It is possible that part is embrittled due to the fact that surface is exposed to a corrosive environment for a long period of time. Further discussion on this is provided in the later part of the report.

3.2 General observation (after cleaning with Alconax)

The most important observation after cleaning with Alconax is that there is clear evidence of exfoliation corrosion. Alocanx solution mainly etches the corrosion product and gives better information about the surface. It is believed that ultrasonic cleaning in Alconax solution for 30 min gives ample time to remove all the corrosion products, and more than 30 min does not help in cleaning. Figure 11(a, b) shows an image taken from zone 2 and zone 4 respectively, which illustrates the intergranular corrosion in the LT direction, typical of exfoliation.

Cleaning the fracture surface with Alconax proved beneficial in exposing the finer details of the fracture surface. Figure 11 (c and d) from the region “zone 2” and “zone 4”, respectively, shows fatigue striations that were almost destroyed by the corrosion. Additional micrographs of the fracture surfaces after cleaning with Alconax are given in ***Appendix C***.

SEM analysis on the fracture surface clearly indicates the following features: (a) exfoliation corrosion and (b) fatigue striations. Though exfoliation corrosion is one factor in addition to fatigue striations, it is possible that fatigue may not be the main root cause for the crack propagation. Leaves observed on both fracture surfaces and on the sides indicate that the cracks run parallel to the fracture surface mainly in the LT direction (refer Fig. 5 a-d, Fig. 8c) suggesting exfoliation corrosion, and, fatigue could be a synergistic factor for crack propagation. In general, aluminum alloys, especially 7000 series, are more susceptible to exfoliation corrosion when they are under-aged or peak aged (T6 Temper)[1-4]. The sensitivity to exfoliation depends mainly on the grain orientation, heat treatment, principal stress direction and environment. Intergranular corrosion which is a severe form of exfoliation corrosion occurs mainly due to difference in electrode potential between the grain interior and grain boundary. The presence of intermetallic inclusions in the grain boundary and segregation of solute particles like Cu and Mg

increase this electrode potential by making it more susceptible for corrosion[5]. The solute segregation or gradient is more likely to be the case for underaged and T6 tempered condition. On the other hand in the overaged condition, the concentration gradient of the solutes between the grain boundary and grain interior is reduced and there by the material is less susceptible for corrosion. However, presence of intermetallic inclusions in the grain boundary will increase defects (dislocations) due to the lattice mismatch between the grain and inclusions which again would increase the electrode potential. In addition, copper rich intermetallic particles are nobler compared to the remainder of the alloy and function as cathode[5]. Thus creating a picture of a small cathode and large anode galvanic cell, this is a worse scenario. To further get an insight into the root cause of this failure, microstructural investigation was carried out in LS and ST directions. Samples from zone 1& 2 were cut using a low speed saw and polished using standard metallographic techniques. Polished specimens were then etched using Keller's reagent and observed in Nikon Epiphot 300 inverted optical microscope. In addition, hardness and electrical conductivity measurements was also carried out on the polished specimens. Microstructural, hardness and electrical conductivity studies is expected to provide material property/temper condition.

4. Optical Microstructural Analysis

A 3D view of the microstructure of the specimen with its orientation is given in Figure 12 and a schematic section and its orientation with respect to extrusion direction is illustrated in ***Appendix D***. The microstructure shows elongated grains and flow lines in the LT and LS directions. Intermetallic inclusions are aligned in the extrusion direction and mostly in the intergranular region and are clearly seen in the both LT (Figure 13) and LS (Figure 14) directions. Presence of inclusions in the intergranular region forms a potential path for crack propagation and exfoliation corrosion. Polished and etched specimens showing leaves in the cross section of the fracture surface are shown in ***Appendix E***. Though the microstructure appears to be normal in the LT and LS directions, careful observation indicates that there is something abnormal with this microstructure in the ST direction. In the ST direction, the microstructure reveals variation in the grain size and morphology across the surface. Equiaxed recrystallized grains are found in the outer edge and cast dendrite structure (remnant cast structure in the form of skewed dendrites) progressively increased towards the center. Detailed microstructure analysis is given in the

Appendix F. In the region well away from the edge, the microstructure reveals grains with different bright and dark contrast at low magnification as shown in Fig 15a. At high magnification, the micrograph clearly reveals fine skewed dendrites as shown in Fig 15b. The fracture has occurred in the region where the dendrites or cast structure is observed.

The presence of cast structures is common in thick wrought products. However, in the present case, it is quite strange to find in this extruded product whose section thickness is quite small (~ 5 mm or 1.96 in). In wrought products, the cast structure can occur under following processing conditions: thick sections, too low or high processing temperature.

The cast structures need not necessarily come from the grain itself, but can occur in the form of chromium, Cr rich precipitates when homogenization treatment was not complete. Evidence of Cr rich precipitates (dendritic coring) in the form of cast structures is reported in 85% reduced AA7079 – T6 forging components that resulted from high forging temperature (low residual strain)[6]. Though the present subject material is expected to be AA7075-T6, the microstructural defect i.e. dendritic coring is compared with AA7079 – T6 in the literature. This is because, the operating mechanism during structural change from cast to wrought are same in all metals, also true for aluminum alloys irrespective of the grade. Since the dendrites are skewed, the processing temperature could be high enough to accommodate larger strain, especially in the thick section or region away from the die contact. Near the die contact region the strain is large and one can expect recrystallized grain (***Appendix F***). Thus, the observed cast structure resulted from an improper secondary processing condition. As most of the properties are correlated to the microstructure, the properties of the observed structure will be different than the standard properties for this alloy.

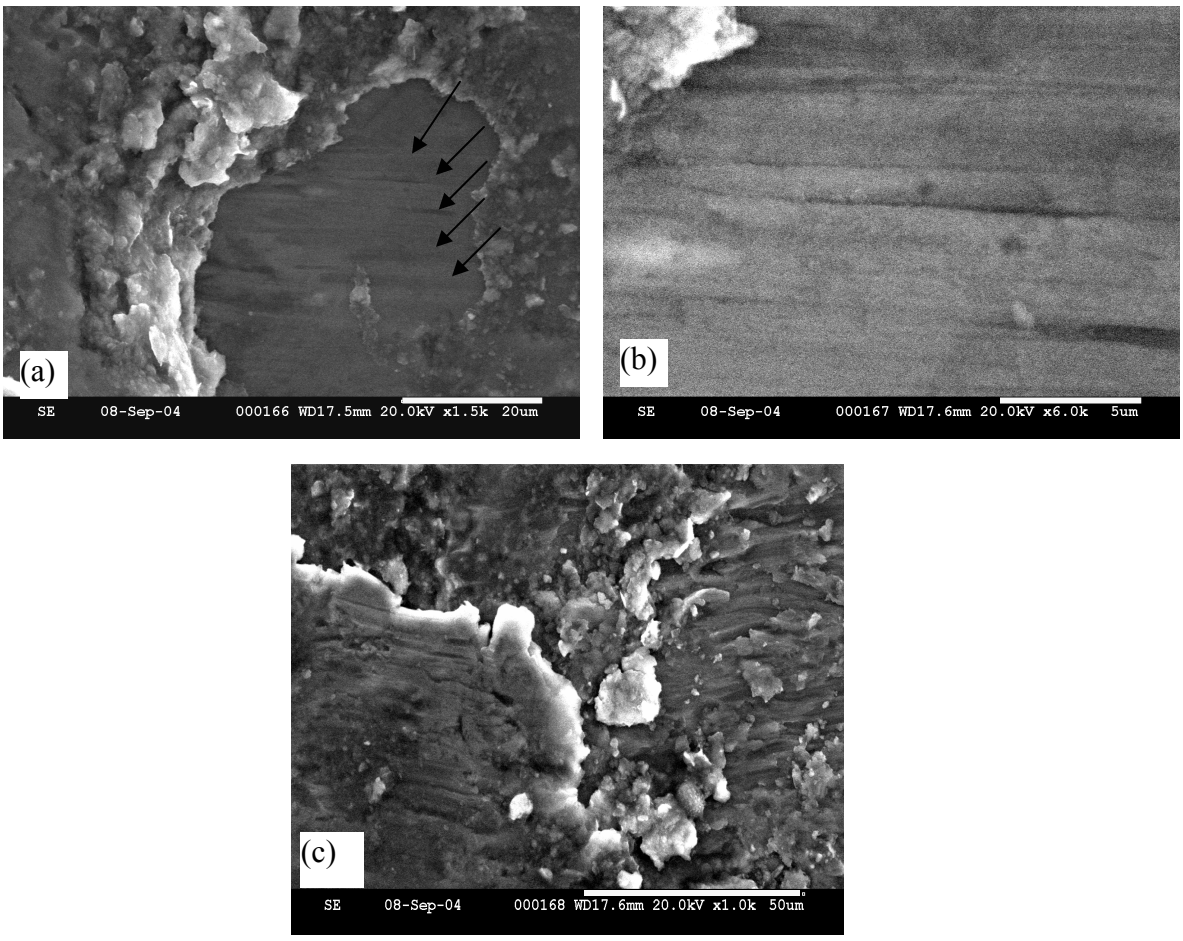

Figure 9: Possible fatigue striations observed in zone 2 - 5: (a) Striations partially covered by corrosion products, striations shown by arrows; (b) high magnification of the same region, and (c) striations observed in zone 2 surface extensively damaged by oxides.

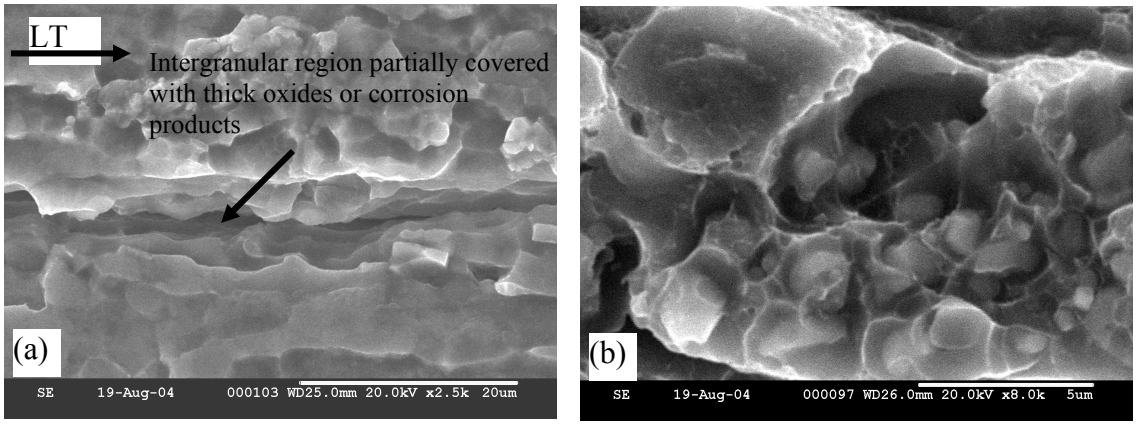

Figure 10: High magnification from (a) corroded region and (b) overload stress rupture.

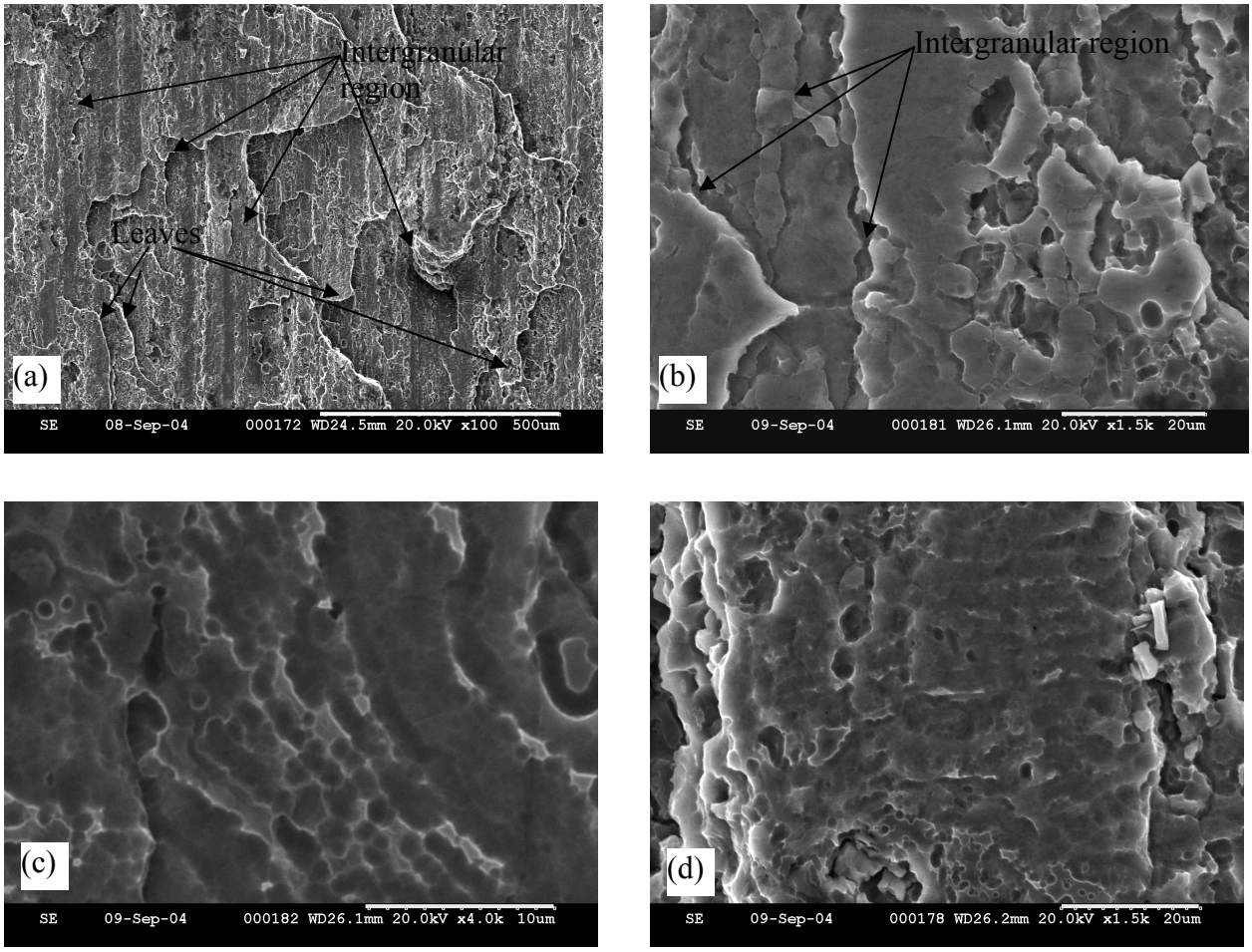

Figure 11: SEM micrograph of the Alocnax cleaned fracture surface taken from (a) zone-2 and (b) Zone-4 clearly shows multiple leaves either partially or completely broken, and several intergranular cracks. Arrow indicates the grain boundary separation region during intergranular fracture. And (c, d) fatigue striations exposed after Alconax cleaning.

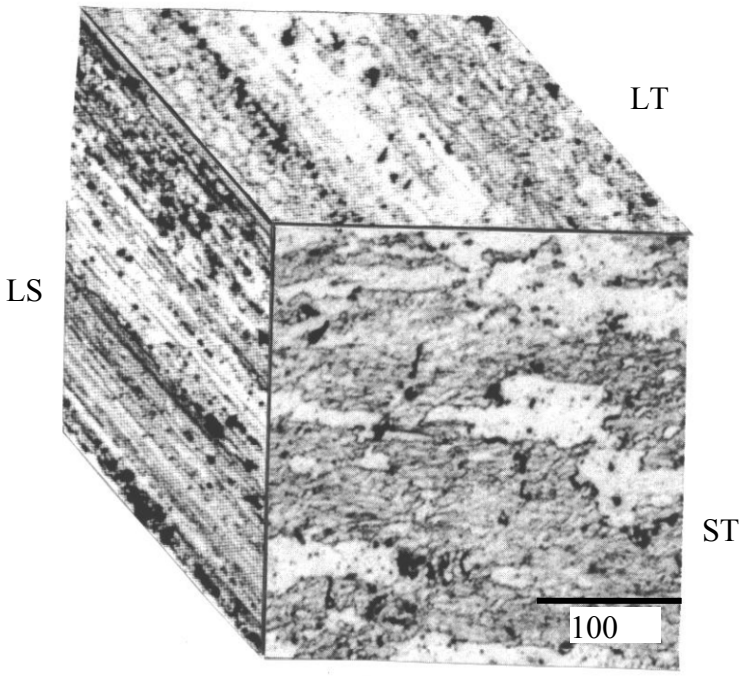

Figure 12: A 3D view of the microstructure with its orientation.

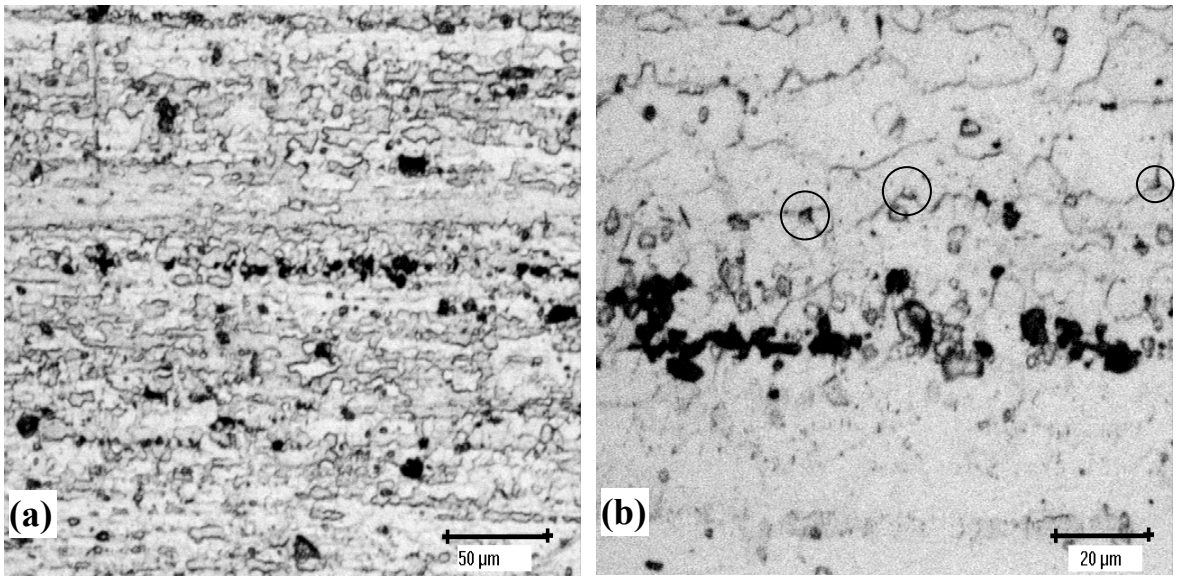

Figure 13: (a) Low and (b) high magnification optical microstructure in LT directions shows intermetallic inclusions aligned in the extrusion direction and in the intergranular region. Inclusion particle in the triple junction, is shown inside circles

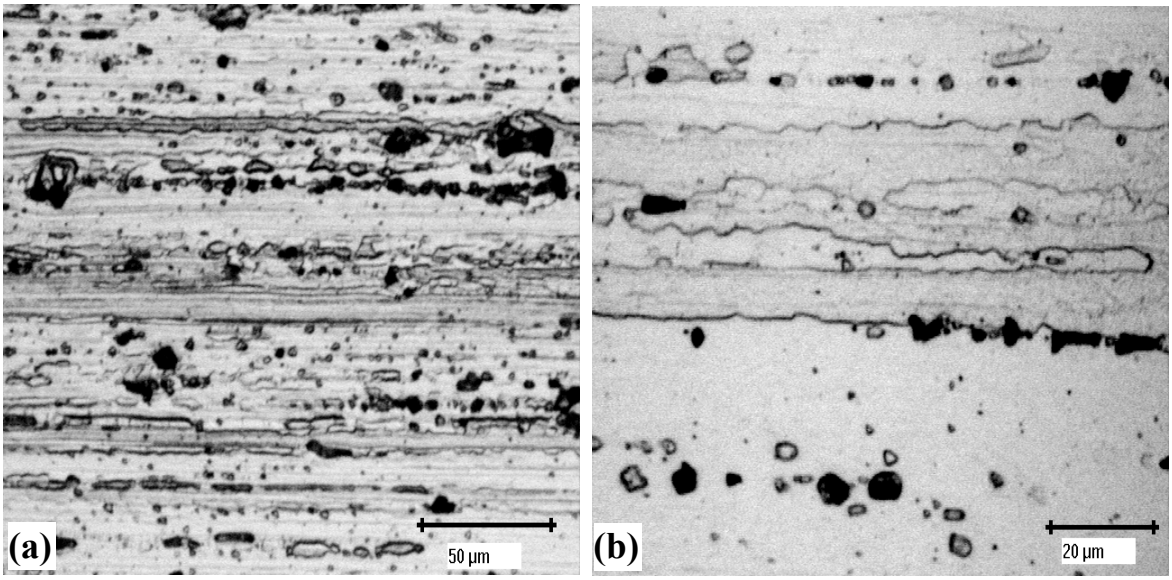

Figure 14: (a) Low and (b) high magnification optical microstructure in LS directions shows intermetallic inclusions aligned in the extrusion direction and in the intergranular region.

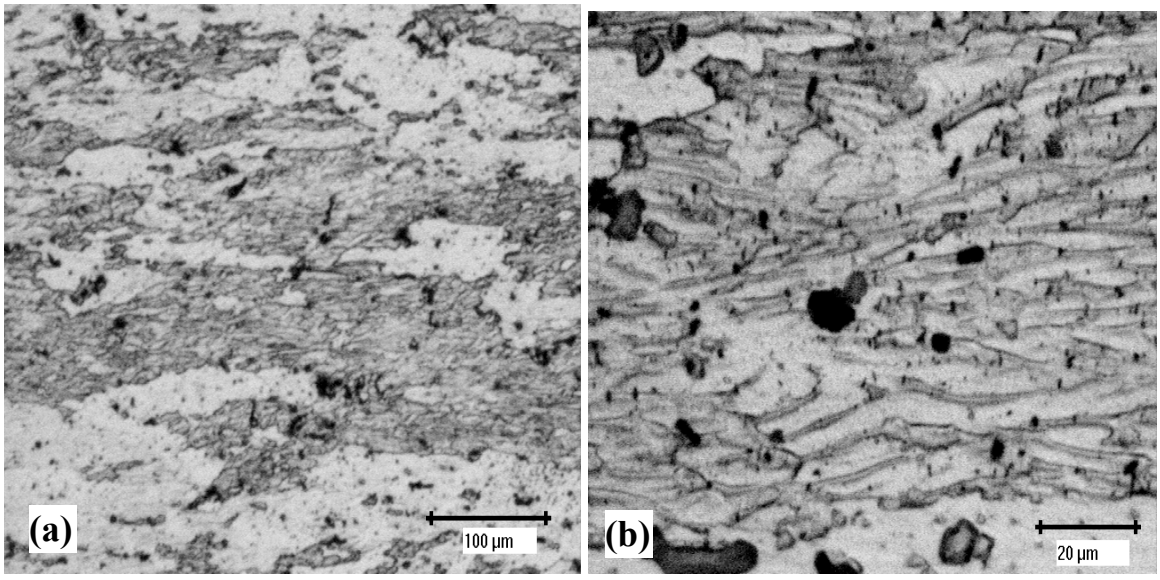

Figure 15: (a) Low and (b) high magnification optical microstructure in ST directions shows intermetallic inclusions aligned in the extrusion direction and in the intergranular region

5. Hardness and Electrical Conductivity Measurements

Hardness and electrical properties were measured from the polished specimen and are given in Table 1 and 2 and compared with the standards. The measured hardness value was about 140 HB, which is slightly low compared to the normal 7075 Al – T6 tempered condition. Similarly, the electrical conductivity which strongly depends on the temper condition, as well as on the microstructure showed very low value (25 % IACS) compared to the expected range (33% IACS) in this material. A low electrical conductivity value is usually observed in cast materials, thus supporting the observed microstructure in the ST direction is the cast one (refer Fig. 15b).

Table 1. Hardness data measured from sectioned specimen and compared with standard

Material	Hardness (HB)
7075 - 0 temper	60[7]
7075 – T6, T651 temper	150[7]
7075 – current material	138 – 140

Table 2. Electrical conductivity measured from sectioned specimen and compared with standard.

Material	Electrical conductivity (% IACS)
7075 – T6, T651, T652 tempers	33[8]
7075 – T76, T7651 tempers	38.5[8]
7075 – T73, T7351, T7352 tempers	40[8]
7075 – current material	25

6. Conclusion

The present investigation on the failure analysis of the part from the C-130 clearly shows the exfoliation corrosion and fatigue. Metallurgical defects due to higher processing temperatures during extrusion are the main root cause for the failure.

7. References

1. Andreatta F, Terryn H and de Wit J.H.W: Corrosion behavior of different tempers of AA7075 aluminum alloy, Electrochimica Acta: Vol. 49, (17/18), July 2004, p. 2851.

2. J. T. Staley, S.C. Byrne, E. L. Colvin and K.P. Kinnear: Corrosion and stress corrosion of 7XXX-W products, Materials Science Forum, Vols. 217-222, 1996, p. 1587.

3. N.C. Bellinger, J. P. Komorowski, M. Liao, D. Carmody, T. Foland and D. Peeler: Preliminary study into the effect of exfoliation corrosion on aircraft structural integrity, 6Th Joint FAAA/DoD/NASA aging aircraft conference, Sept. 16-19, 2002, p.1.

4. ASM Handbook, Fractrography, Vol. 12, 9th edition, p. 28.

5. R.G. Buchheit, R.K. Boger, M. C. Carroll, R.M. Leard, C. Paglia and J.L. Searles: The electrochemistry of intermetallic particles and localized corrosion in Al alloys, Journal of Metals, July 2001, p. 29.

6. Metals handbook, vol. 9, 9th edition, p. 367.

7. Metals handbook, vol. 2, 9th edition, p. 130.

8. Metals handbook, vol. 2, 9th edition, p. 131.

Appendix A: Supplemental Images

Macroscopic images

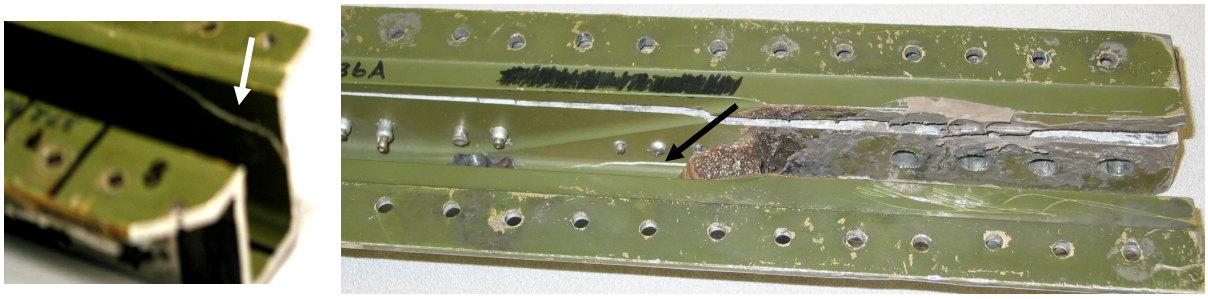

Figure A 1: Multiple cracks observed in the as received part are shown below prior to cutting the parts.

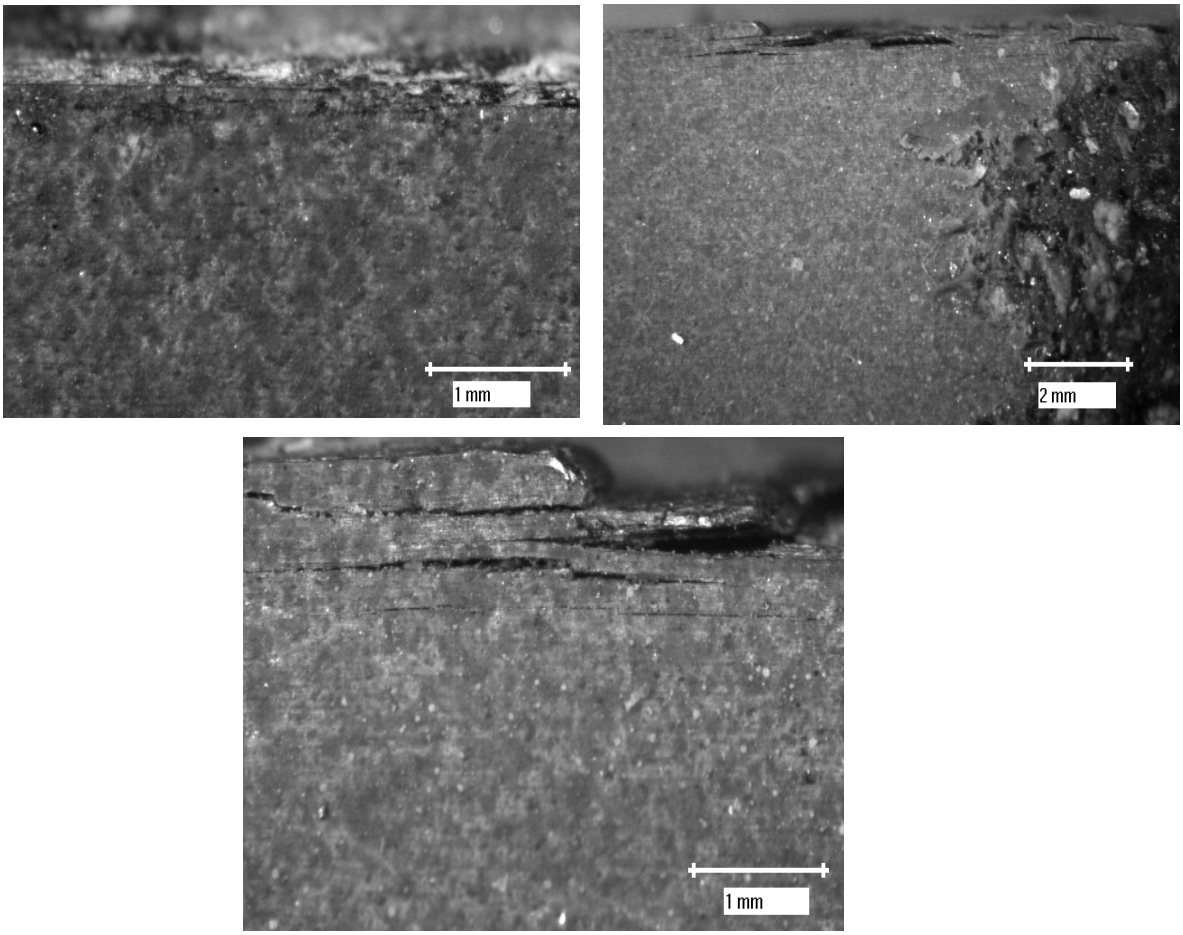

Figure A 2: Exfoliation additional photomicrographs

Appendix B: EDAX Data

EDAX analysis was done in the cross section of the fracture surface and three analysis reports are given in this appendix. Elemental analysis showed sodium content varied from 2.5 to 4.0 wt. %, sulfur 4.9 to 6.2 wt. % and oxygen 0 – 20.3%. EDAX spectrum, elemental composition in wt. 5 and corresponding micrograph are also provided.

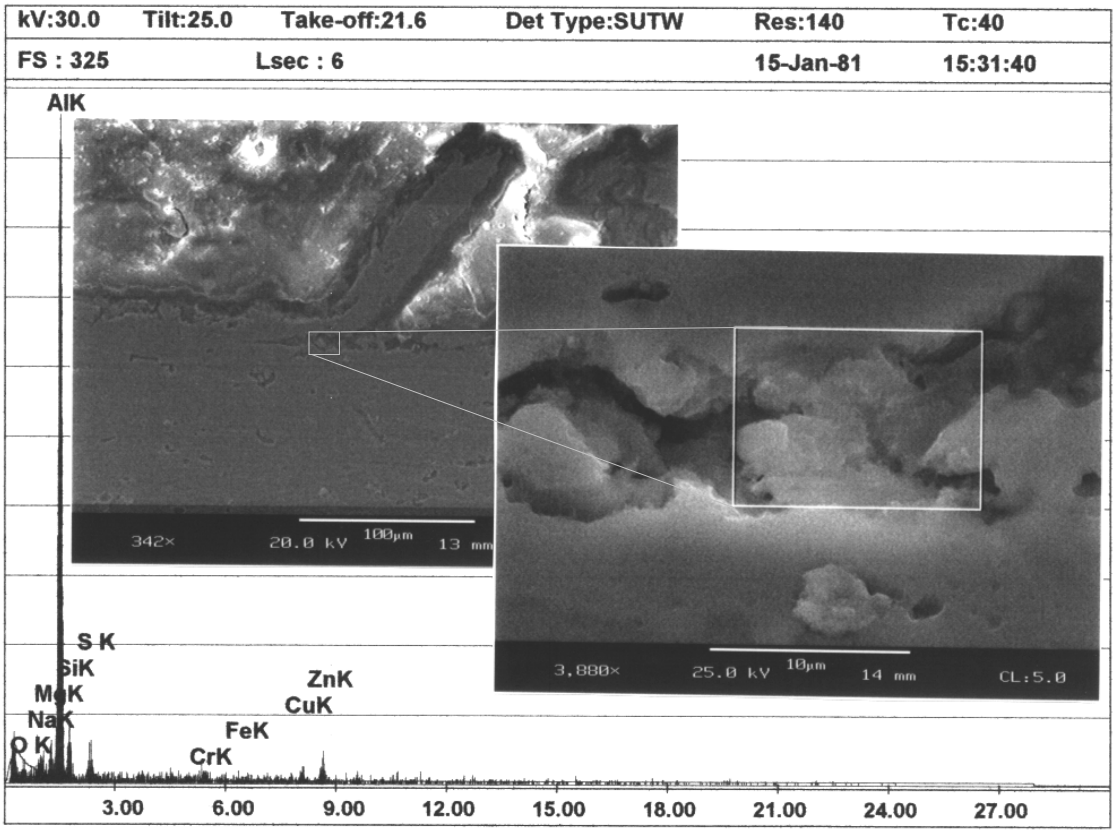

Element	Wt %
O K	0.00
NaK	2.46
MgK	3.51
AlK	66.49
SiK	13.82
S K	5.72
CrK	0.83
FeK	0.50
CuK	2.48
ZnK	4.19
Total	100.00

Figure B 1: The SEM micrograph shows the cross section of the fracture surface with clear exfoliation type corrosion. High magnification of the rectangular box represents the region from where the area analysis was done. Circular region shows the region where the subsequent analysis was done.

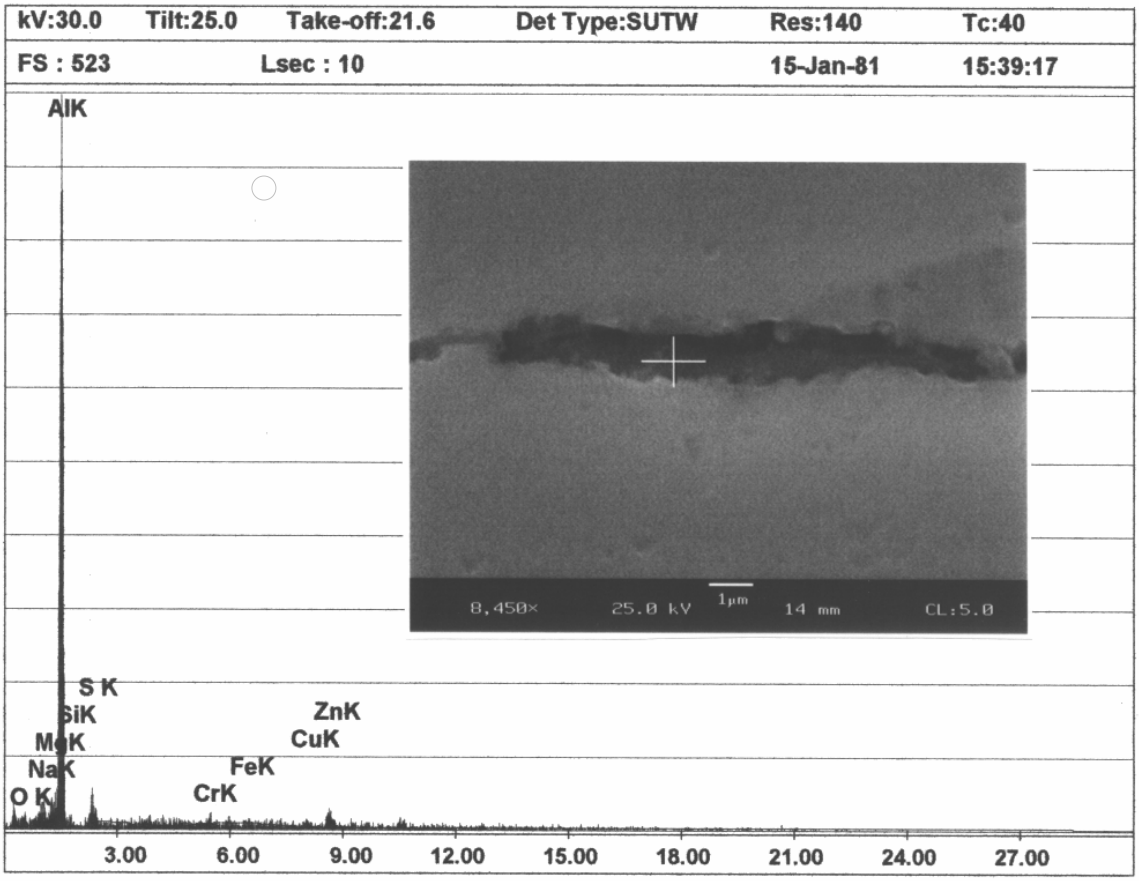

Element	Wt %
O K	10.08
NaK	3.07
MgK	3.24
AlK	69.16
SiK	2.32
S K	4.88
CrK	0.92
FeK	0.18
CuK	1.34
ZnK	4.81
Total	100.00

Figure B 2: EDAX spot analysis taken on a crack below the fracture surface. SEM micrograph shows the cross section of the fracture surface at high magnification. EDAX analysis was done in crack tip below the fracture surface. Cross symbol represents the spot analysis area. The exact location of this crack is shown in the previous micrograph as a circular region.

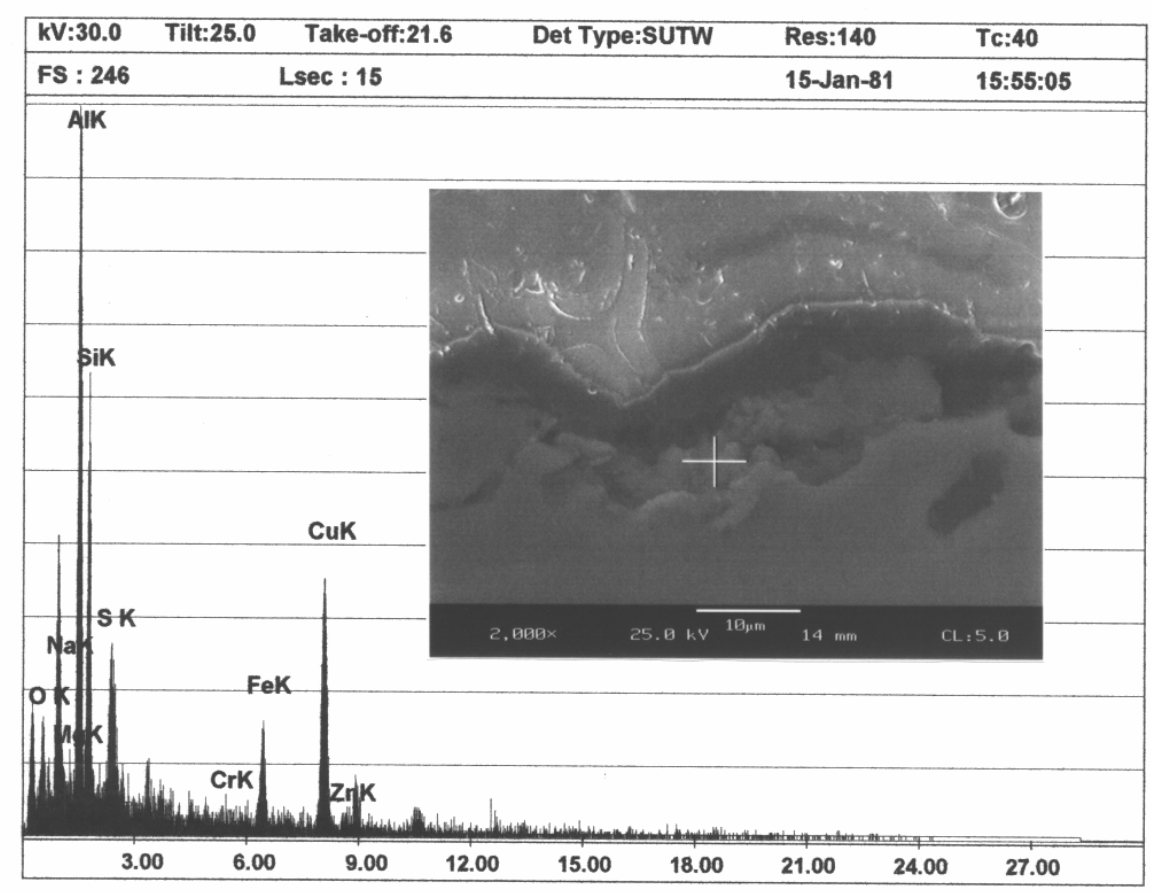

Element	Wt %
O K	20.27
NaK	4.05
MgK	0.94
AlK	27.66
SiK	19.42
S K	6.24
CrK	0.52
FeK	3.97
CuK	15.34
ZnK	1.59
Total	100.00

Figure B 3: EDAX spot analysis taken on the fracture surface. SEM micrograph shows the cross section of the fracture surface. EDAX analysis is taken on the fracture top surface. Cross symbol represents the spot analysis area.

Appendix C: SEM micrographs after cleaning with Alconax

SEM micrographs of the fracture surface after cleaning with Alconax are shown below from different zones. Intergranular (IG) corrosion is seen clearly from these micrographs.

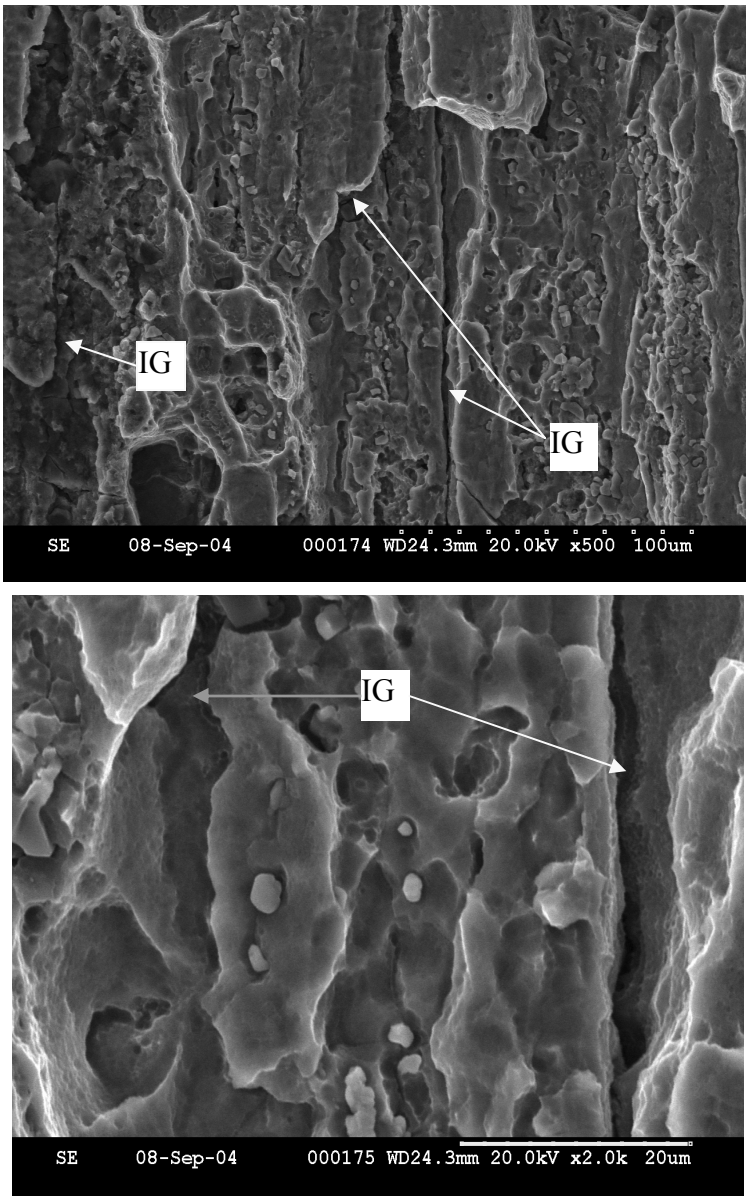

Figure C 1: SEM micrographs of the fracture surface after cleaning with Alconax are shown below from Zone 2.

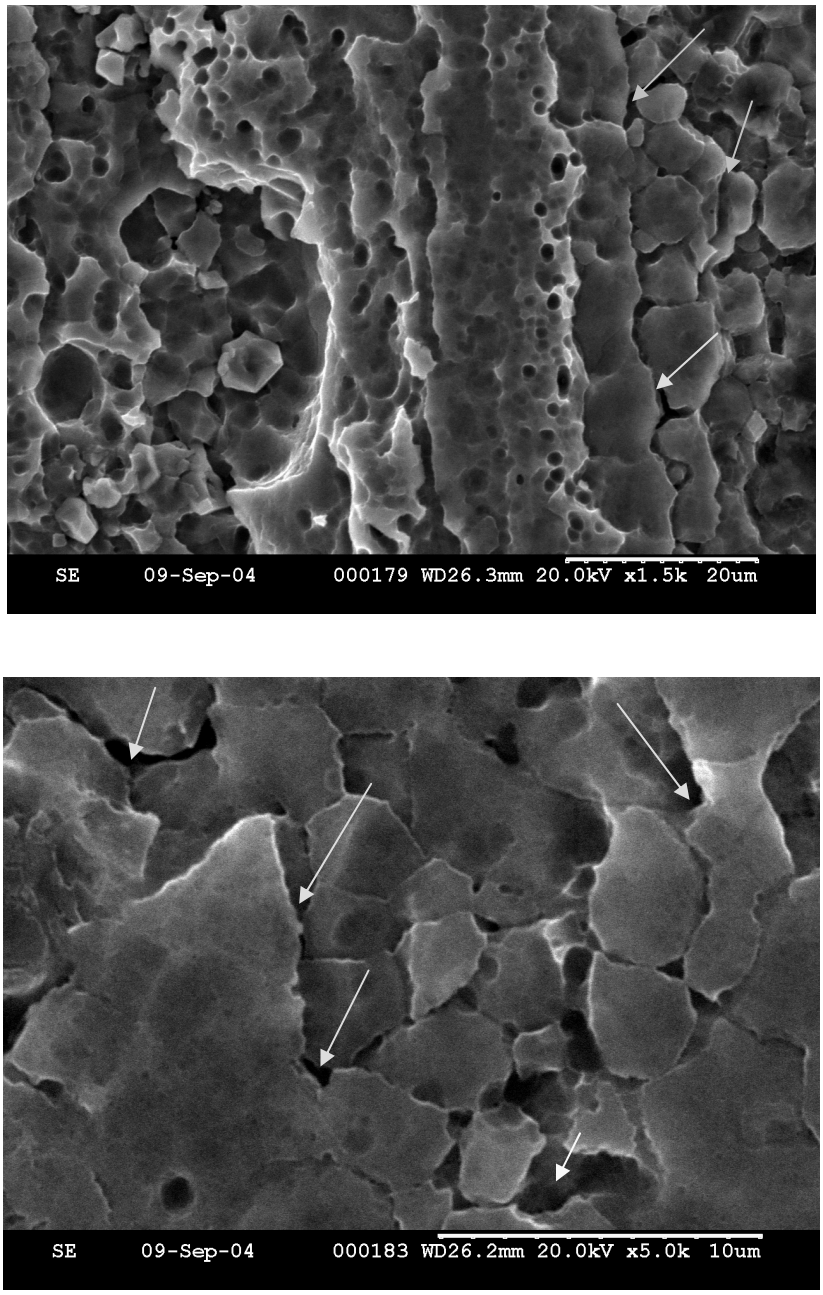

Figure C 2: SEM micrographs of the fracture surface after cleaning with Alconax are shown below from Zone 4. Arrows indicates the intergranular region attacked severely by corrosion environment. The corrosion products are completely etched by cleaning in Alconax solution. Compare these micrographs with Figure 8 (b & d).

Appendix D: Component Schematics

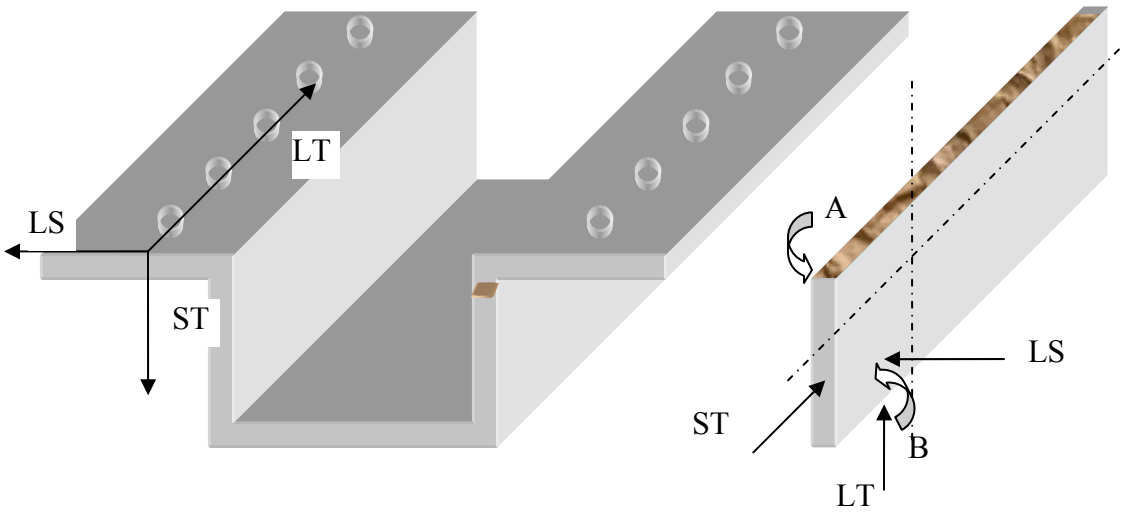

Figure D 1: Schematic sectioning from the sample for optical microscopy.

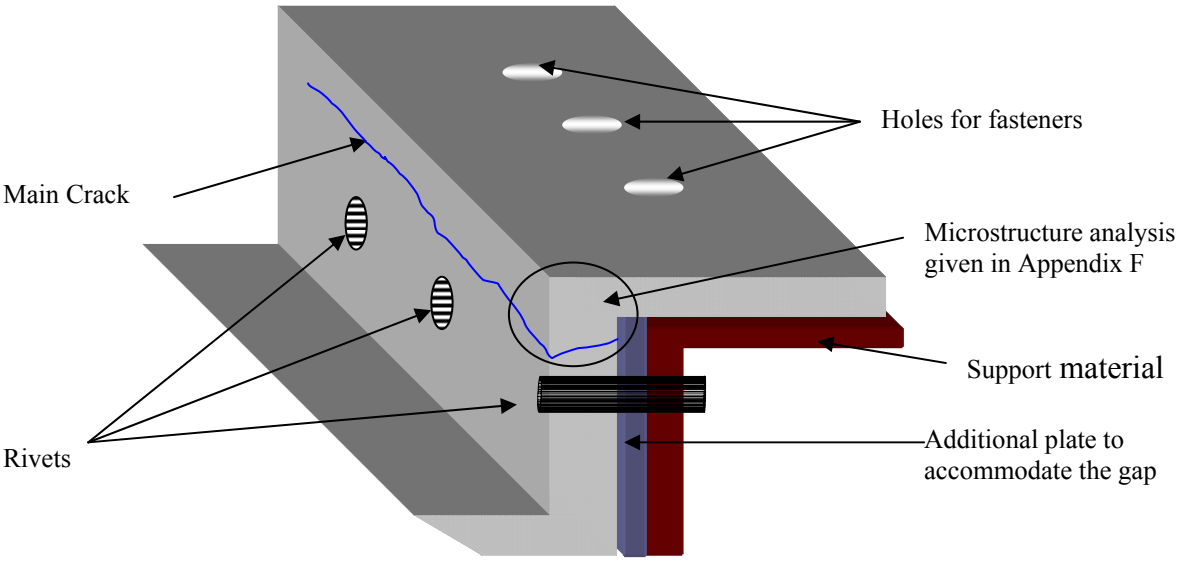

Figure D 2: Schematic of repair and possible imposition of tensile stress from the additional plate and support. Microstructural analysis of the circular region is given in Appendix F.

Appendix E: Photomicrographs of Polished and Etched Specimens.

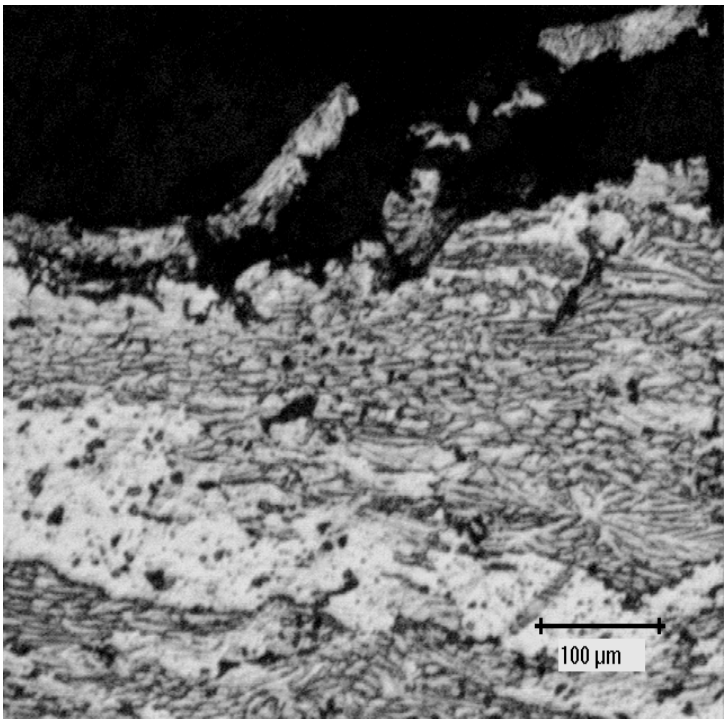

Figure E 1: Leaves seen in the cross section of the fracture surface in ST direction.

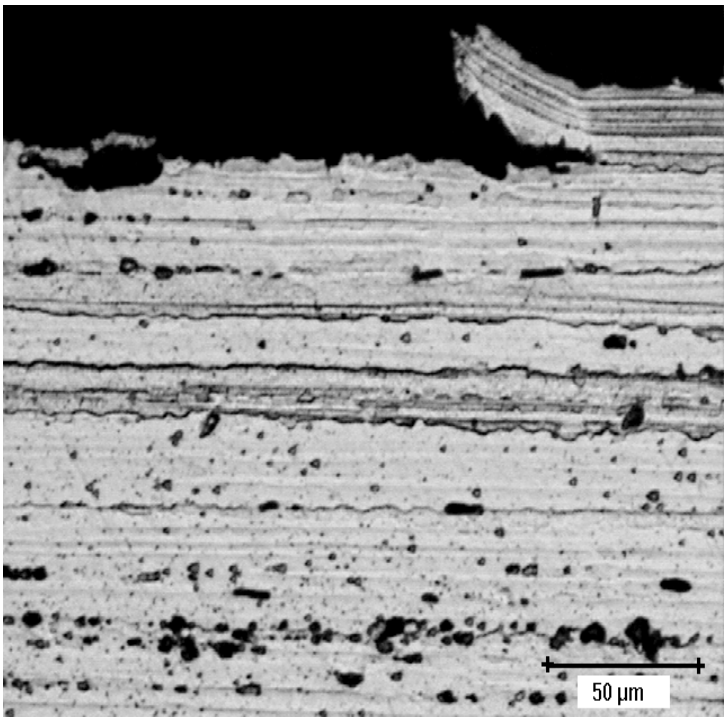

Figure E 2: Leaves seen in cross section of the fracture surface in LT direction.

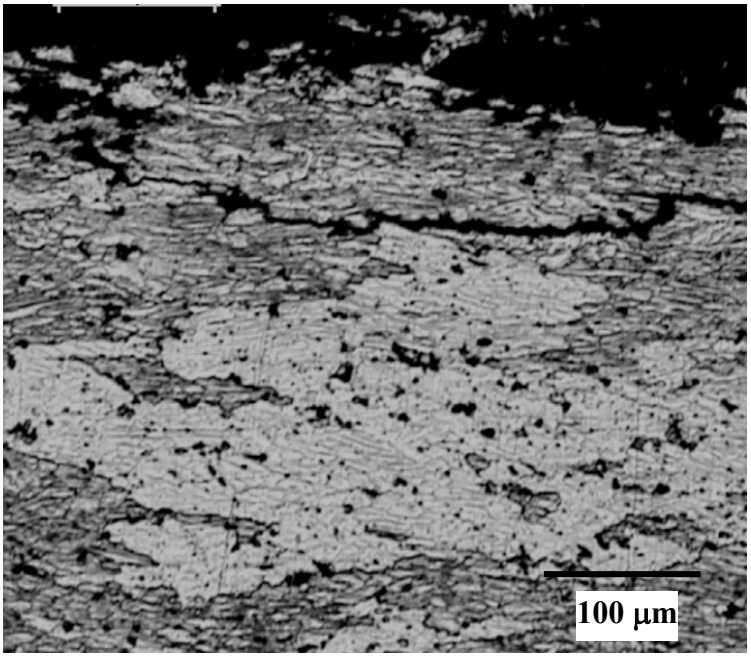

Figure E 3: Cross section of the fracture surface in ST direction. Dendritic structure is clearly visible even at low magnification.

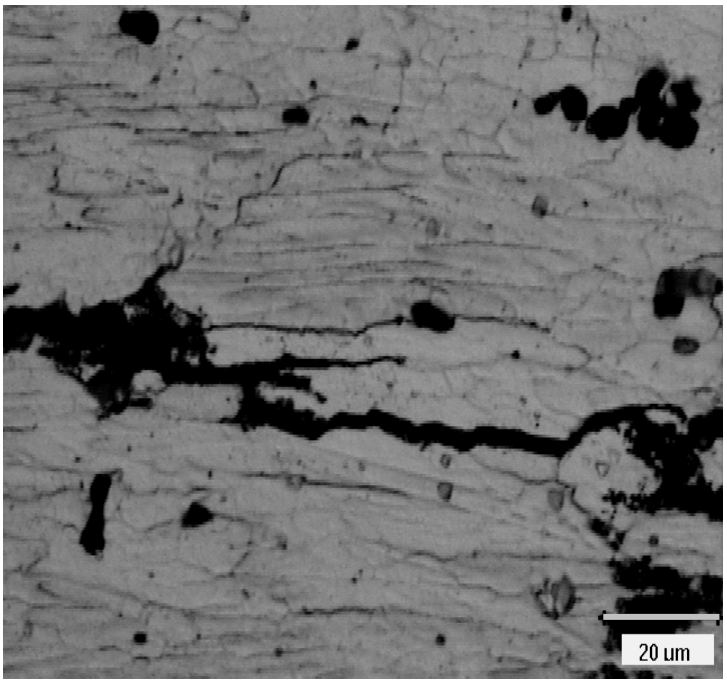

Figure E 4: Intergranular corrosion running along the inter-dendrite region.

Appendix F: Variation in the grain size though the section thickness

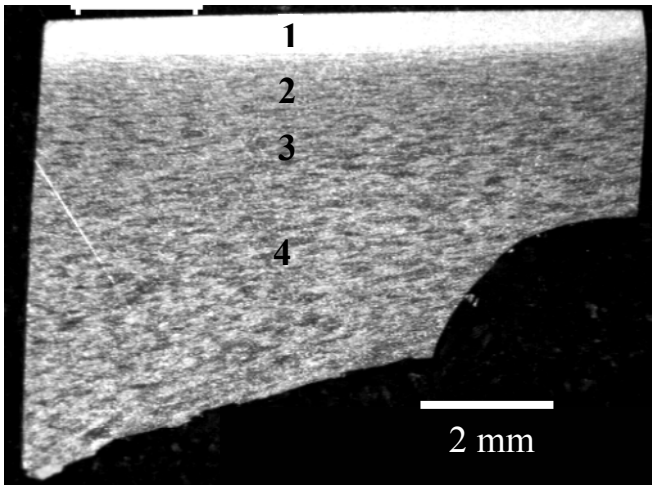

Figure F 1: Micrograph of circular region from Figure D2 indicating regions in subsequent micrographs from this Appendix.

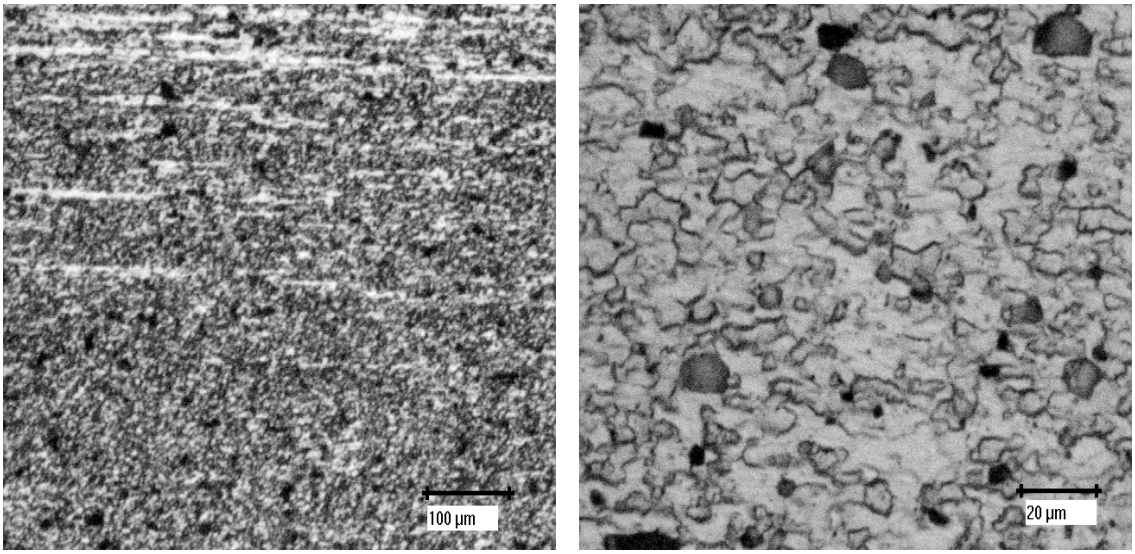

Figure F 2: Region 1- low and high magnification optical micrographs near the edge where there is large strain due to contact with die.

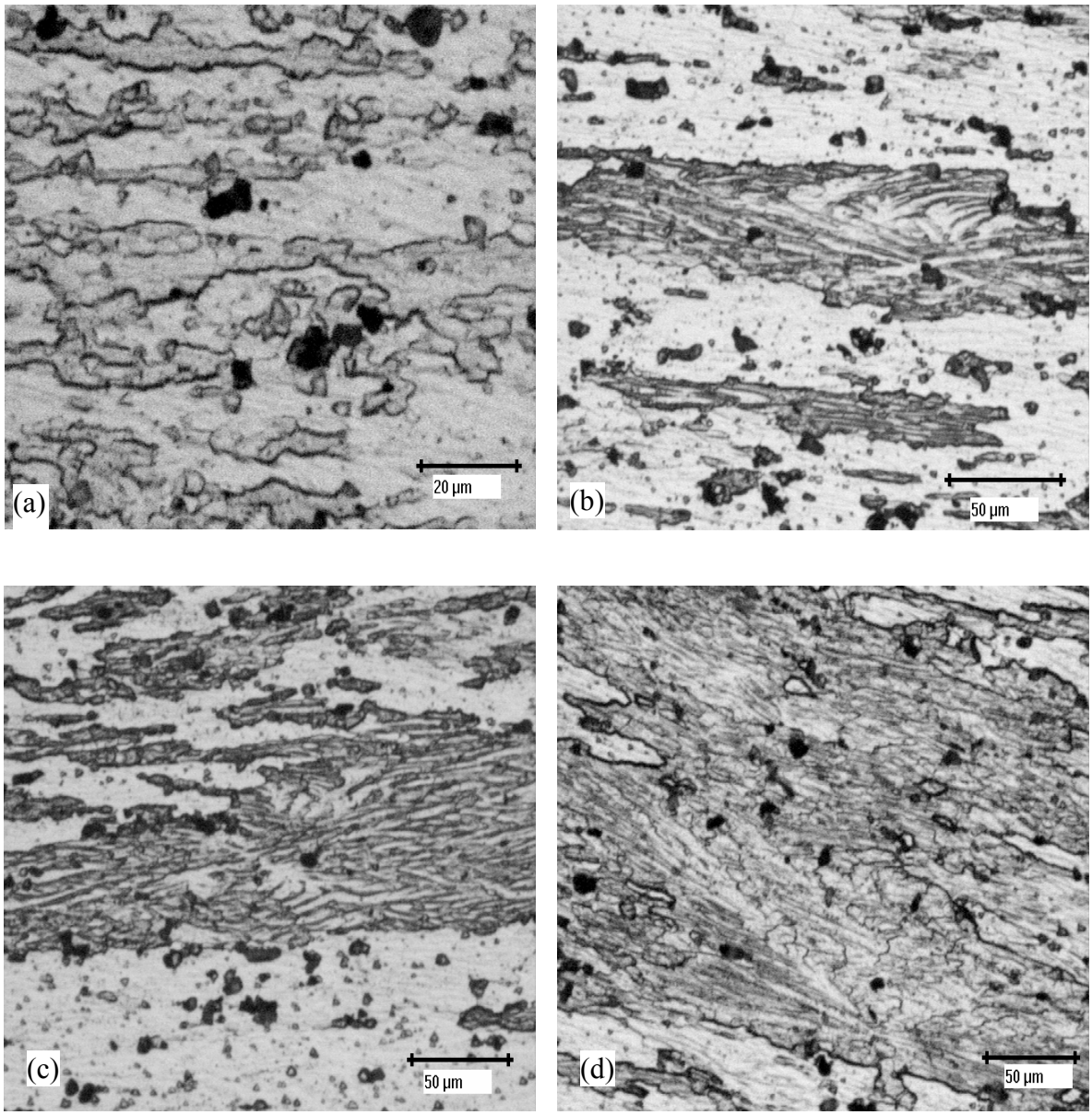

Figure F 3: Optical micrographs of a) Region 2 b) Region 3 and c, d) Region 4 as described by Figure F1.

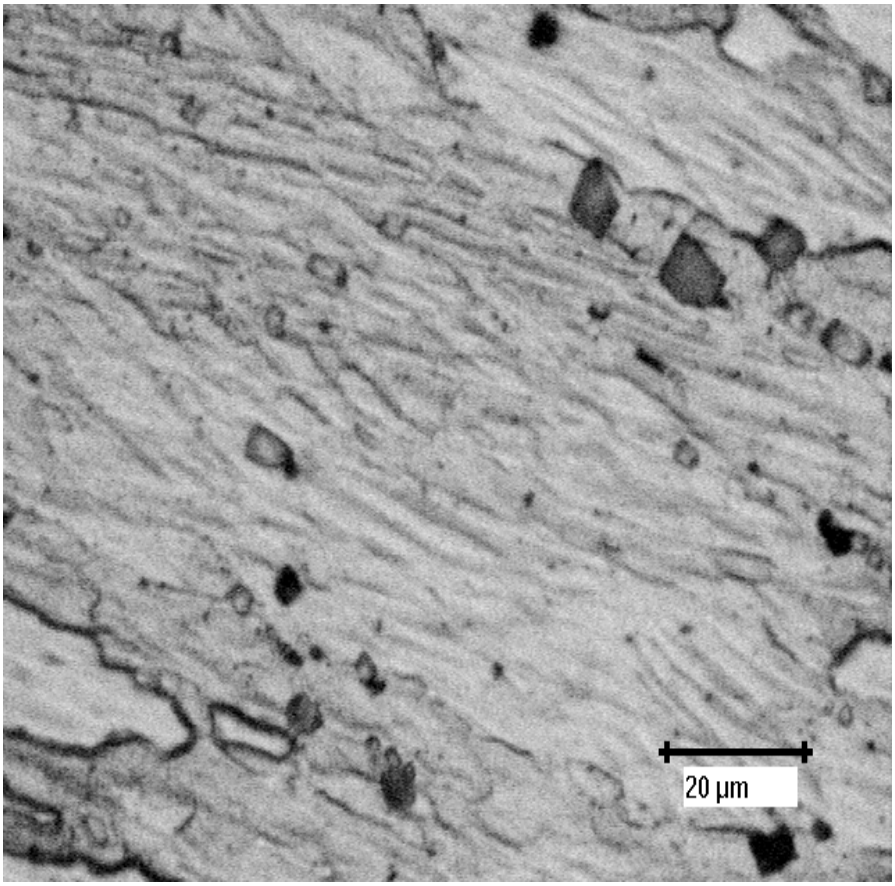

Figure F 4: Optical micrographs of Region 4 - high magnification.